The interferon-inducible GTPase MxB promotes capsid disassembly and genome release of herpesviruses

Manutea C. Serrero[1,2], Virginie Girault[3], Sebastian Weigang[4], Todd M. Greco[5], Ana Ramos-Nascimento[1], Fenja Anderson[1], Antonio Piras[3], Ana Hickford Martinez[1], Jonny Hertzog[6], Anne Binz[1,2,7], Anja Pohlmann[1,2,7], Ute Prank[1], Jan Rehwinkel[6], Rudolf Bauerfeind[8], Ileana M. Cristea[5], Andreas Pichlmair[3,9], Georg Kochs[4], and Beate Sodeik[1,2,7]

[1] Institute of Virology, Hannover Medical School, Hannover, Germany
[2] RESIST - Cluster of Excellence, Hannover Medical School, Hannover, Germany
[3] Institute of Virology, Technical University Munich, Munich, Germany
[4] Institute of Virology, Freiburg University Medical Center, University of Freiburg, Freiburg, Germany
[5] Department of Molecular Biology, Princeton University, Princeton, USA
[6] MRC Human Immunology Unit, MRC Weatherall Institute of Molecular Medicine, Radcliffe Department of Medicine, University of Oxford, Oxford, UK
[7] German Center for Infection Research (DZIF), Hannover-Braunschweig Partner Site, Germany
[8] Research Core Unit Laser Microscopy, Hannover Medical School, Hannover, Germany
[9] German Center for Infection Research (DZIF), Munich Partner site, Germany

Corresponding author:
Beate Sodeik
Institute of Virology, OE 5230
Hannover Medical School
Carl-Neuberg-Str. 1, D-30623 Hannover, Germany
Phone: ++49 - 511 - 532 2846
FAX: ++49 - 511 - 532 8736
Email: sodeik.beate@mh-hannover.de

Number of pages: 47
Number of figures: 8 figures, 8 supplementary figures, 4 supplementary tables

ABSTRACT

Host proteins sense viral products and induce defence mechanisms, particularly in immune cells. Using cell-free assays and quantitative mass spectrometry, we determined the interactome of capsid-host protein complexes of herpes simplex virus and identified the large dynamin-like GTPase myxovirus resistance protein B (MxB) as an interferon-inducible protein interacting with capsids. Electron microscopy analyses showed that cytosols containing MxB had the remarkable capability to disassemble the icosahedral capsids of herpes simplex viruses and varicella zoster virus into flat sheets of connected triangular faces. In contrast, capsids remained intact in cytosols with MxB mutants unable to hydrolyse GTP or to dimerize. Our data suggest that MxB senses herpesviral capsids, mediates their disassembly, and thereby restricts the efficiency of nuclear targeting of incoming capsids and/or the assembly of progeny capsids. The resulting premature release of viral genomes from capsids may enhance the activation of DNA sensors, and thereby amplify the innate immune responses.

INTRODUCTION

Infections with human alphaherpesviruses are associated with painful and stigmatizing manifestations such as herpes labialis or herpes genitalis, but also cause life-threatening meningitis or encephalitis, potentially blinding eye infections, herpes zoster, and post-herpetic neuralgia, particularly in immunocompromised patients (Gershon *et al.*, 2015; Whitley & Roizman, 2016; Whitley & Johnston, 2021). Herpes simplex viruses (HSV-1, HSV-2) and varicella zoster virus (VZV) productively infect epithelial and fibroblast cells of the skin and mucous membranes as well as neurons, but are restricted in immune cells. Macrophages, Langerhans cells, dendritic cells, and NK cells mount potent immune responses against alphaherpesviruses (Whitley & Roizman, 2016).

Intracellular DNA sensors are crucial to sense herpesvirus infections, and to induce caspase-1 mediated inflammation and type I IFN expression (Hertzog & Rehwinkel, 2020; Kurt-Jones *et al.*, 2017; Lum & Cristea, 2021, Ma *et al.*, 2018; Paludan *et al.*, 2019; Stempel *et al.*, 2019). During an unperturbed infection, capsid shells shield herpesviral genomes from cytosolic sensors during nuclear targeting as well as after nuclear genome packaging (Arvin & Abendroth, 2021; Döhner *et al.*, 2021; Knipe *et al.*, 2021). HSV-1 capsids can withstand compressive forces of up to 6 nN which is more than sufficient to endure the 18 atm repulsive pressure of the packaged viral DNA (Bauer *et al.*, 2013; Roos *et al.*, 2009). So far, it is unclear how cytosolic DNA sensors gain access to herpesviral genomes; either cytosolic host factors disassemble the sturdy herpesviral capsids during infection, or the nuclear envelopes become leaky.

HSV-1 virions contain an amorphous tegument layer that links the icosahedral capsids with a diameter of 125 nm to the viral envelope proteins (Crump, 2018; Dai & Zhou, 2018; Diefenbach, 2015). To identify cytosolic proteins that promote or restrict infection by interacting with HSV-1 capsids, we have developed cell-free methods to reconstitute capsid-host protein complexes using tegumented capsids from extracellular viral particles or tegument-free capsids from the nuclei of infected cells (Radtke *et al.*, 2014). Intact capsids are incubated with cytosol prepared from tissues or cultured cells, and the capsid-host protein complexes are isolated, and characterized by mass spectrometry (MS), immunoblot, electron microscopy, and functional assays. We could show that

74 HSV-1 capsids require inner tegument proteins to recruit microtubule motors, to move along
75 microtubules, to dock at nuclear pore complexes (NPCs), to release viral genomes from capsids, and
76 to import viral genomes into the nucleoplasm, and that capsids lacking tegument cannot move along
77 microtubules, but still bind to nuclear pores (Anderson *et al.*, 2014; Ojala *et al.*, 2000; Radtke *et al.*,
78 2010; Wolfstein *et al.*, 2006).

79 Here, we searched for proteins that might contribute to sensing cytosolic capsids and thereby
80 promote the detection of herpesviral genomes. Using extracts of matured THP-1 cells, a model
81 system for human macrophages (Tsuchiya *et al.*, 1980), we identified type I interferon (IFN) inducible
82 proteins that bound specifically to HSV-1 capsids. Among them was the large dynamin-like GTPase
83 myxovirus resistance protein B (MxB). MxB limits the infection of several herpesviruses, and can
84 mediate almost 50% of the IFN-mediated restriction of HSV-1, although its mode of action has
85 remained elusive so far (Crameri *et al.*, 2018; Liu *et al.*, 2012; Schilling *et al.*, 2018; Vasudevan *et al.*,
86 2018). MxB has been first described for its potent inhibition of HIV infection (Goujon *et al.*, 2013;
87 Kane *et al.*, 2013; Liu *et al.*, 2013). The human *MX2* gene codes for a full-length MxB (residues 1-715)
88 and a smaller version (residues 26-715) that lacks an N-terminal extension (NTE), which both are
89 highly expressed upon IFN induction (Melen *et al.*, 1996). MxB likely operates as an anti-parallel
90 dimer but can also form higher-order filaments; its N-terminal GTPase domain connects to a bundle
91 signalling element that moves relative to the GTPase domain in response to nucleotide binding, and
92 the C-terminal stalk domain is critical for MxB oligomerization (Alvarez *et al.*, 2017; Chen *et al.*, 2017;
93 Fribourgh *et al.*, 2014; Gao *et al.*, 2011).

94 We show here that both, full-length MxB(1-715) and MxB(26-715) have the remarkable property
95 to disassemble the capsids of the three human alphaherpesviruses HSV-1, HSV-2, and VZV, so that
96 they can no longer transport nor shield the viral genomes. Capsid disassembly did not require
97 proteases but depended on the ability of MxB to hydrolyse GTP and to dimerize. As the large
98 tegument protein pUL36 links the capsid vertices to the other tegument proteins (Crump, 2018; Dai
99 & Zhou, 2018; Diefenbach, 2015), and as an increasing amount of associated tegument proteins
100 protected capsids against MxB mediated disassembly, we propose that MxB attacks the capsids at

their vertices. Our data suggest that MxB can bind to and disassemble incoming as well as progeny capsids, and thereby might increase the sensing of cytosolic and nuclear viral genomes. Therefore, the MxB GTPase might be the sought-after capsid destroyer that acts upstream of cytosolic or nuclear sensors to promote viral genome detection and induction of innate immune responses.

RESULTS

IFN induction prevents HSV-1 infection of macrophages. Before investigating capsid interactions with macrophage proteins, we compared HSV-1 infection in human keratinocytes (HaCat), pigment epithelial cells (RPE), and THP-1 cells at low, moderate or high multiplicity of infection (MOI). We stimulated monocyte THP-1 cells with phorbol 12-myristate 13-acetate to differentiate them into a macrophage-like phenotype, and used them either directly (Mϕ) or after a resting period of 3 days ($M\phi_R$). HSV-1 replicated productively in HaCat and RPE cells up to 20 hpi, while a pre-treatment with IFN delayed and reduced but did not prevent the production of infectious virions (Fig. 1). Both Mϕ and $M\phi_R$ released 10 to 100-fold less infectious HSV-1, and an IFN pre-treatment prevented infection at all MOIs. Thus, Mϕ and $M\phi_R$ restricted HSV-1 infection efficiently, and the induction of IFN-stimulated genes (ISGs) prevented any productive infection.

IFN-induced protein changes in the cytosol of macrophages. To identify cytosolic macrophage proteins that might foster or restrict HSV-1 capsid functions, we prepared extracts from $M\phi_R$ or IFN-induced $M\phi_{IFN}$ to reconstitute capsid-host protein complexes as they might assemble in macrophages (Fig. S1). Using subcellular fractionation and subsequent dialysis (Fig. S2A), we depleted the extracts of nuclei and mitochondria (Fig. S2B; pellet P1), cytoplasmic membranes such as Golgi apparatus, endoplasmic reticulum and plasma membrane (P1, P2), and small metabolites (S2, S3, S4). Furthermore, most of the cytoskeletal tubulin and actin sedimented into the first pellet (P1), while glyceraldehyde 3-phosphate dehydrogenase (GAPDH), a bona-fide cytosolic protein, remained soluble in the supernatants (S1, S2, S2', S3, S4). Next, we analysed the proteomes of the $M\phi_R$ and IFN-induced $M\phi_{IFN}$ cytosols at low ATP/GTP concentration [ATP/GTP^{low}] by mass spectrometry (MS; Table S1). We detected 494 (Fig. S2C; black circles) of more than 600 reported IFN-inducible proteins

(Rusinova *et al.*, 2013). Of those, GALM, COL1A1, LGALS3BP, NT5C3A, IFI44, IFIT2, IFIT3, GBP4, SRP9, IFIT5, DSP, and L3HYPDH were enriched by at least 2-fold in the $M\phi_{IFN}$ cytosol (Fig. S2C; red). These changes might reflect IFN-induced transcriptional or translational regulation, post-translational modification, subcellular localization, or susceptibility to proteolysis, and show that the IFN induction had changed the cytosol proteome of the $M\phi_{IFN}$.

HSV-1 capsids interact with specific cytosolic macrophage proteins. To search for cytosolic Mϕ proteins whose interactions with HSV-1 capsids depend on their surface composition, we generated tegumented viral $V_{0.1}$, $V_{0.5}$, and V_1 capsids as well as D capsids with a reduced tegumentation (Fig. S1). For this, we lysed extracellular particles released from HSV-1 infected cells with non-ionic detergent to solubilize the envelope proteins and lipids, and in the presence of 0.1, 0.5, or 1 M KCl to modify intra-tegument protein-protein interactions (Anderson *et al.*, 2014; Ojala *et al.*, 2000; Radtke *et al.*, 2010; Radtke *et al.*, 2014; Wolfstein *et al.*, 2006; Zhang & McKnight, 1993). Furthermore, we dissociated tegument from $V_{0.1}$ capsids by a limited trypsin digestion to generate so-called D capsids. We then incubated similar amounts of different capsid types as calibrated by immunoblot for the major capsid protein VP5 (Fig. S2D) with cytosol at ATP/GTP^{low} from $M\phi_R$ or IFN-induced $M\phi_{IFN}$ for 1 h at 37°C. The capsid-host protein complexes assembled *in vitro* were harvested by sedimentation, and their interactomes were determined by quantitative MS (c.f. Fig. S1). As before (Radtke *et al.*, 2010; Snijder *et al.*, 2017), the protein intensities were normalized across samples to the abundance of the major capsid protein VP5 (Table S2, host; Table S3, viral).

Of 2983 proteins identified (Table S2), we detected 1816 in at least 3 of the 4 replicates in any of the 8 different capsid-host protein complexes. Of those, 598 host proteins bound differentially to one capsid type over another (Table S2; fold change ≥ 2.8; permutation-based FDR ≤ 0.05). The HSV-1 capsids had recruited specifically 279 proteins of $M\phi_R$ and 390 of $M\phi_{IFN}$ cytosol of which 71 were shared. Hierarchical clustering analyses of the associated $M\phi_R$ or $M\phi_{IFN}$ proteins identified 4 major classes; e.g. one enriched on V over D capsids (Fig. S3A and S3B, top green) and one enriched on D over V capsids (Fig. S3A and S3B, bottom violet). Therefore, we compared the capsid-host interactions of D capsids directly to $V_{0.1}$ (Fig. 2A, 2D), $V_{0.5}$ (Fig. 2B, 2E), or V_1 (Fig. 2C, 2F) capsids, and

identified 82 proteins of $M\phi_R$ (Fig. 2A, 2B, 2C) and 141 of $M\phi_{IFN}$ (Fig. 2D, 2E, 2F) with 35 being shared (Table S2; difference ≥ 2.83-fold; FDR ≤ 0.01). The $M\phi_R$ capsid-host complexes included 12 and the ones of $M\phi_{IFN}$ 19 proteins listed in the interferome database (Rusinova *et al.*, 2013; red in Fig. 2). Gene ontology and pathway enrichment analyses showed that the identified 82 $M\phi_R$ (Fig S4) and 141 $M\phi_{IFN}$ (Fig. 3) proteins included many players of innate immunity, intracellular transport, nucleotide and protein metabolism, as well as intracellular signalling. Overall, the host proteomes of $V_{0.1}$ (red) and D (grey) capsids were rather distinct, but more similar for $V_{0.5}$ (blue) and V_1 (green) capsids (Fig. S4 and Fig. 3). For example, $V_{0.1}$ capsids had recruited specifically the innate immunity proteins PIGR, IGHA1, BPIFA1 and DEFA3, but D capsids LRRFIP1, UFC, C3 and DCD from $M\phi_R$ cytosol. In $M\phi_{IFN}$, the D capsids were enriched for C3, C6, IGBP1, UBA5, UBXN1, UBE3A, and RNF123. These data suggest that protein domains displayed on different capsids interacted with specific cytosolic $M\phi_R$ or $M\phi_{IFN}$ proteins.

In these assays, the capsids interacted with several proteins already validated to promote or restrict HSV or VZV infection. Examples are the ESCRT-III co-factor VPS4 (Cabrera *et al.*, 2019; Crump *et al.*, 2007), EIF4H (Page & Read, 2010), the Kif2a subunit of kinesin-13 (Turan *et al.*, 2019), the POLR1C subunit of RNA polymerase III (Carter-Timofte *et al.*, 2018), the DNA protein kinase PRKDC (Justice *et al.*, 2021), and DDX1 (Zhang *et al.*, 2011). Moreover, the deubiquitinase USP7 (Rodriguez *et al.*, 2020) and the ubiquitin ligases RNF123, TRIM72, UFC1 and UBE3A as well as the proteasome might regulate capsid functionality (Huffmaster *et al.*, 2015; Schneider *et al.*, 2021) or their degradation(Horan *et al.*, 2013; Sun *et al.*, 2019). These data show that HSV-1 capsids exposing a different tegument composition recruited specific cytosolic proteins from resting or IFN-induced macrophages.

HSV-1 capsids recruit specific proteins responding to or regulating type I IFN. We next analysed the $M\phi_{IFN}$ samples in detail as IFN induction had prevented HSV-1 infection completely. We generated cluster maps for the 32 capsid-associated proteins belonging to the GO clusters *Response to type I IFN* or *Regulation of type I IFN production* (Table S2). V capsids recruited DHX9, HSPD1 and FLOT1 as well as proteins involved in the DNA damage response like PRKDC/DNA-PK, XRCC5, and

XCCR6 from both, $M\phi_R$ and $M\phi_{IFN}$ cytosol (Fig. 4). Interestingly, V capsids bound specifically to STAT1 in $M\phi_R$, but to ADAR and IFIT2 in $M\phi_{IFN}$ cytosol. D capsids were enriched for IFI16, OAS2, POLR1C, STAT2, and MxB in $M\phi_{IFN}$ but not in $M\phi_R$ (Fig. 4, Fig. S5). Particularly, the discovery of MxB in these capsid-host protein complexes was interesting, as MxB but not its homolog MxA restricts infections of the herpesviruses HSV-1, HSV-2, MCMV, KSHV, and MHV-68, but its mode of action has not been elucidated (Crameri *et al.*, 2018; Liu *et al.*, 2012; Schilling *et al.*, 2018; Vasudevan *et al.*, 2018). Therefore, we investigated the interaction of human MxB with HSV-1 capsids further.

MxB binds to capsids. We first characterized the MxB fractionation behaviour during the cytosol preparation (Fig. S2). As reported (Goujon *et al.*, 2013; Melen *et al.*, 1996), MxB was upregulated in IFN-induced $M\phi_{IFN}$. MxB sedimented with nuclei and mitochondria as expected (Cao *et al.*, 2020), with cytoplasmic membranes, and possibly filamentous MxB (Alvarez *et al.*, 2017) might have been sedimented too. Both, after the addition of ATP and GTP (ATP/GTP^{high}) or the hydrolase apyrase (Pilla *et al.*, 1996; ATP/GTP^{low}), a significant fraction of MxB remained soluble in the cytosol.

Next, we confirmed by immunoblotting that MxB co-sedimented with HSV-1 capsids which had been incubated in cytosols from $M\phi_R$ or $M\phi_{IFN}$. In line with the MS results, MxB bound better to D than to $V_{0.1}$, $V_{0.5}$, or V_1 capsids (Fig. 5A). We next probed authentic nuclear capsids, namely empty A, scaffold-filled B, or DNA-filled C capsids, as well as tegumented V_1, $V_{0.5}$, $V_{0.1}$ or D capsids with cytosol of A549-MxB(1-715) epithelial cells expressing MxB(1-715). Nuclear A and C as well as V_1 and D capsids recruited MxB efficiently, while B, $V_{0.1}$ and $V_{0.5}$ capsids bound less MxB (Fig. 5B). MxB did not sediment by itself, and also did not associate with agarose beads used as another sedimentation control (Fig. 5A, 5B). These data indicate that MxB binds to specific structural features on the capsid surface.

In cells, MxB mediated restriction of herpesvirus replication depends on its N-terminal 25 amino acid residues (NTE), its GTPase activity, and its capacity to form dimers (Crameri *et al.*, 2018; Schilling *et al.*, 2018; Vasudevan *et al.*, 2018). We incubated capsids with cytosols containing MxA, MxB(1-715), MxB(26-715) (Melen *et al.*, 1996; Melen & Julkunen, 1997), MxB(K131A) with reduced GTP binding, MxB(T151A) lacking the GTPase activity, or MxB(M574D) unable to dimerize (Alvarez *et al.*,

2017; Fribourgh *et al.*, 2014; King *et al.*, 2004; Schilling *et al.*, 2018). In contrast to MxA, MxB(1-175), MxB(26-715), and MxB(M574D) co-sedimented with capsids to a similar extent. Interestingly, MxB(K131A) did not bind to capsids, while MxB(T151A) bound even stronger (Fig. 5C). These data suggest that conformational changes associated with GTP binding or hydrolysis contribute to MxB interaction with HSV-1 capsids.

MxB disassembles capsids of alphaherpesviruses. Next, we tested whether MxB might affect HSV-1 capsid stability. While the previous capsid sedimentation assays were performed at ATP/GTP^{low}, they suggested that the GTP/GDP state of MxB might modulate its interaction with capsids. To test this experimentally, we supplemented the cytosols with 1 mM GTP, 1 mM ATP, and 7.5 mM creatine phosphate to maintain high ATP/GTP levels [ATP/GTP^{high}]. We resuspended sedimented capsid-host protein complexes and applied them onto EM grids (Fig. S1), or we added isolated capsids directly onto EM grids and then placed them on a drop of cytosol to allow the formation of capsid-host protein complexes (Fig. 6A). This direct *on-grid assay* required 50 times fewer capsids than the *sedimentation-resuspension assay* and allowed for time-course analyses. For both, we negatively contrasted the samples with uranyl acetate and analysed them by electron microscopy.

When capsids were incubated with cytosol from A549 control cells not containing MxB, we saw mostly intact capsids with an appropriate diameter of about 125 nm, and an intact icosahedral morphology characterized by pentons at the vertices and hexons on the triangular capsid faces (Fig. 6B). The capsids contained genomic DNA as the uranyl acetate used for negative contrast staining had not or only partially entered the capsid lumen. But a treatment with cytosol from IFN-induced Mϕ_{IFN} or A549-MxB(1-715) cells dramatically impaired the capsid shell. Based on different MxB induced morphological changes, we classified the capsid structures that we had identified by immunolabeling for capsid proteins (Fig. S6) into three categories. *Intact capsids* (Fig. 6B, Fig. S6A) have an icosahedral morphology and include empty A, scaffold-filled B, and DNA-filled C capsids. *Punched capsids* are characterized by indentations on one or more vertices and an impaired icosahedral shape (Fig. 6C, Fig. S6B). *Flat shells* have completely lost their icosahedral shape

(Fig. 6D, Fig. S6C). We estimated the number of capsomers on *flat shells* based on their area, and scored a structure with <100 capsomers as a half capsid and with ≥100 as one capsid (numbers in Fig. 6D). Cytosols containing MxB(1-715) also disassembled capsids of HSV-2 (not shown) or VZV (Fig. 6E) to *punched capsids* and *flat shells*. As MxB induced capsid disassembly of HSV-1, HSV-2 and VZV, these experiments suggest that MxB restricts the infection of herpesviruses by targeting their capsids.

MxB requires GTP hydrolysis and dimerization to attack herpesviral capsids. Next, we further characterized the capsid disassembly activity of MxB by quantitative electron microscopy. Cytosol from IFN-induced $M\phi_{IFN}$ disassembled more than 80% of the capsids within 1 h while resting $M\phi_{R}$ disassembled only about 40% (Fig. 7A). Cytosol derived from A549 control cells had a minor effect on capsids, while cytosol from A549-MxB(1-715) cells disassembled capsids almost as efficiently as cytosol from $M\phi_{IFN}$. Spiking cytosol from A549 control cells with an increasing percentage of A549-MxB(1-715) cytosol led to an increasing capsid disassembly with a majority of *punched capsids*, at 50% or 66% MxB cytosol, while incubation in pure A549-MxB(1-715) cytosol lead to more than 95% disassembly to mostly *flat shells* within 1 h of incubation (Fig. 7B). We then asked whether MxB had activated other host proteins to mediate capsid disassembly, or whether it was directly responsible. We prepared cytosol from A549-MxB(1-715)-MxB(26-715) expressing both untagged MxB proteins, or from A549-MxB-FLAG expressing MxB(1-715)-FLAG and MxB(26-715)-FLAG. Both cytosols promoted capsid disassembly (MxB; MxB-FLAG in Fig. 7C), but an immunodepletion with anti-FLAG antibodies removed the FLAG-tagged MxB proteins (Fig. S7), and accordingly the disassembly activity from the A549-MxB-FLAG cytosol (MxB-FLAG FT), while the anti-FLAG did neither deplete untagged MxB proteins, nor affect the capsid disassembly activity of the A549-MxB(1-715)-MxB(26-715) cytosol (MxB FT).

We next tested at ATP/GTP^{high} the effect of various MxB mutants on HSV-1 capsid stability. While full-length MxB(1-715) induced capsid disassembly, the MxB mutants impaired in GTPase activity (T151A), GTP binding (K131A), or dimerization (M574D) as well as cytosol with MxB at ATP/GTP^{low} did not (Fig. 7D). In contrast, the smaller MxB(26-715) protein lacking the NTE retained about 50% of the

capsid disassembly activity. Furthermore, studying the stability of capsids pre-adsorbed *on-grid* in a time-course revealed a lag phase of about 30 min until broken capsids appeared with increasing rate (Fig. 7E). The percentage of *punched capsids* reached a plateau at 50 min, while the amount of *flat shells* continued to increase (Fig. 7E). Further experiments showed that MxB attacked D capsids more efficiently than tegumented $V_{0.5}$ capsids, of which about 70% resisted the MxB attack (Fig. 7F). In contrast, the $V_{0.1}$ capsids seemed to be spared from MxB attack, since no broken capsids appeared within an 1 h treatment. Since MxB restricts infection of several herpesviruses (Crameri *et al.*, 2018; Liu *et al.*, 2012; Schilling *et al.*, 2018; Vasudevan *et al.*, 2018), we compared the impact of MxB on D capsids from HSV-1(17^+)Lox, HSV-1(KOS), HSV-2(333), or on nuclear C capsids from VZV(rOka). Capsids of these human alphaherpesviruses were all susceptible to MxB attack (Fig. 7G).

MxB attack leads to the release of viral genomes from capsids. Next, we determined how well the capsid shells protected the viral genomes against a DNA nuclease digestion. Capsids released three or two times more viral genomes in cytosols from MxB(1-715) or MxB-FLAG than from control or MxB(M574D) cells (Fig. 7H). Together, these data indicate that the MxB GTPase disassembles the capsid shells and induces a release of viral DNA of several herpesviruses. Our experiments suggest that GTP binding and hydrolysis as well as dimerization contribute to MxB-mediated disassembly of alphaherpesvirus capsids. Its slow start with a lag of about 30 min indicates that the capsid attack might require some nucleating or cooperative reaction to assemble active MxB oligomers or an MxB-containing complex onto capsids.

Tegument proteins protect against MxB attack. As complete tegumentation shielded $V_{0.1}$ capsids against destruction, while MxB bound to surface features exposed on $V_{0.5}$, A, C and D capsids, we compared the proteomes of the $V_{0.1}$, $V_{0.5}$, V_1, and D capsids. We calibrated the relative abundances of the 58 HSV-1 proteins detected to the normalized amounts of the major capsid protein VP5. The tegument compositions of $V_{0.1}$, $V_{0.5}$, and V_1 capsids were similar to each other but different from D capsids (Fig. 8). The bona-fide capsid proteins VP21, VP24, VP22a, VP19c, and VP23 varied little among all capsid types. However, D capsids contain a bit less capsid surface proteins; namely VP26,

the capsid specific vertex components (CSVC) pUL17 and pUL25, and to some extent the portal pUL6, and less of the major tegument proteins VP22, VP13/14, VP16, VP11/12 as well as other tegument proteins with ICP0, pUL36 and pUL37 being most susceptible to the trypsin treatment. Overall, there were little differences in the relative tegument protein amounts among $V_{0.5}$ and V_1 capsids. In contrast, $V_{0.1}$ capsids contained more tegument proteins, e.g. VP13/14, pUS3, pUL41, pUL16, pUS11 and pUL40. All capsid preparations contained traces of membrane proteins and nuclear HSV-1 proteins contributing to DNA replication and packaging (Fig. S8). These data further validated that a treatment with 0.5 or 1 M KCl during the detergent lysis of virions destabilized intra-tegument interactions. Furthermore, the limited trypsin digestion had reduced the capsid proteome further and increased the susceptibility to MxB attack.

DISCUSSION

Cell-type specific defence mechanisms shape the arms race between proteins restricting or promoting nuclear targeting of incoming viral capsids and viral genome release into the nucleoplasm. We have developed biochemical assays to investigate functional interactions of viral capsids with host cell structures (Radtke *et al.*, 2014), and analysed here HSV-1 capsid-host protein complexes assembled in cytosols from resting $M\phi_R$ or IFN-induced $M\phi_{IFN}$ cells. We show that the IFN-inducible MxB GTPase bound to alphaherpesviral capsids, most likely to structural features around the capsid vertices, and disassembled herpesvirus capsids in a GTP-dependent fashion, and so that they no longer shielded the viral genomes. Capsid disassembly by MxB could reduce nuclear targeting of incoming capsids and genomes, but stimulate the activation of cytosolic DNA sensors and innate immune responses.

Cytosolic IFN-induced macrophage proteins binding to HSV-1 capsids. IFN induction prevented HSV-1 infection of Mϕ, and increased the cytosolic abundance of at least 12 proteins listed in the interferome database (Rusinova *et al.*, 2013). Here, we assembled host protein-capsid complexes from HSV-1 capsids and cytosols of Mϕ or $M\phi_{IFN}$ cells as they might also form in cells. While $V_{0.5}$ and V_1 capsids recruited unique but also common proteins, the proteomes of $V_{0.1}$ and D capsids were

more distinct. These results are consistent with immunoelectron microscopy data showing that the surface of distinct V capsid types display different tegument epitopes (Radtke *et al.*, 2010), and with cryoelectron tomography data revealing diminishing tegument densities from $V_{0.1}$, $V_{0.5}$, V_1 capsids to C capsids (Anderson *et al.*, 2014). Accordingly, capsids with different tegument composition recruit distinct sets of cytosolic proteins from brain tissue (Radtke *et al.*, 2010), or macrophages as shown here. Host proteins may bind to viral proteins in both states, when they are soluble in the cytosol or the nucleoplasm, or when they are associated with capsids. From host proteins shown here to bind to capsids, direct interactions with tegument proteins have already been reported; e.g. USP7 binding to ICP0 (Everett *et al.*, 1997) or EIF4H binding to vhs (pUL41; Page & Read, 2010). Furthermore proteins involved in intracellular trafficking or virus assembly associated particularly with tegumented V capsids. For example, importin α5 (*KPNA1*) might mediate capsid targeting to the nuclear pores (Döhner *et al.*, 2018; Döhner *et al.*, 2021), while RAB1B contributes to the envelopment of cytosolic HSV-1 capsids (Zenner *et al.*, 2011).

MxB binding to alphaherpesviral capsids. In addition to MxB, the host-capsid complexes included other antiviral proteins which in turn might be counteracted by HSV-1 proteins. Several $M\Phi_{IFN}$ proteins already know to restrict herpesviruses, e.g. STAT2, POLR1C, IFI16, DDX58 (RIG-I), and OAS2 (Kurt-Jones *et al.*, 2017; Lum & Cristea, 2021; Ma *et al.*, 2018), bound preferentially to D capsids. As it was not known how MxB might restrict herpesviral infection (Crameri *et al.*, 2018; Schilling *et al.*, 2018; Vasudevan *et al.*, 2018), we investigated its association with capsids further. B capsids are less sturdy and have not undergone the structural changes that stabilize the A and C capsids (Roos *et al.*, 2009; Sae-Ueng *et al.*, 2014; Snijder *et al.*, 2017). Intriguingly, this stabilization depends on the CSVC proteins pUL17 and pUL25 (Sae-Ueng *et al.*, 2014; Snijder *et al.*, 2017), which are present on B, A, and C capsids (Anderson *et al.*, 2014; Radtke *et al.*, 2010; Snijder *et al.*, 2017). As MxB bound to A, C and D, but not to B capsids, it might recognize surface features formed during capsid stabilization, e.g. matured CSVCs or portals, which are increasingly shielded on tegumented V_1, $V_{0.5,}$ and $V_{0.1}$ capsids.

MxA and MxB GTPases inhibit several viruses by blocking early steps of infection (Haller *et al.*, 2015). MxB binding to HIV capsids depends on its N-terminal region (NTR) of about 90 residues and the GTPase domain (Betancor *et al.*, 2019; Fricke *et al.*, 2014; Smaga *et al.*, 2019; Xie *et al.*, 2021). Similarly, HSV-1 capsids bound MxB(1-715) and to a lesser extent MxB(26-715). But in contrast to HIV capsids (Betancor *et al.*, 2019; Xie *et al.*, 2021), HSV-1 capsids recruited also the GTPase deficient MxB(T151A) and the monomeric MxB(M574D). These data indicate that the interaction of MxB with HSV-1 capsids depends on the NTE of 25 residues, its GTP/GDP status, but not on its dimerization.

MxB induced disassembly of alphaherpesviral capsids. HSV-1 capsid disassembly did not require proteolysis as the cytosols contained protease inhibitors, but may be modulated by other host proteins as there was a considerable lag phase. MxB did not attack fully tegumented $V_{0.1}$ capsids, while $V_{0.5}$ or D capsids were more susceptible. The large tegument protein pUL36 links other tegument proteins to the capsids; it is tightly associated with pUL17 and pUL25 at the CSVCs at the pentons, and it extends towards the 2-fold symmetry axes connecting neighbouring capsid faces (Coller *et al.*, 2007; Huet et al. 2016; Liu *et al.*, 2019; Newcomb & Brown, 1991; Schipke *et al.*, 2012). Our electron microscopy data suggest that MxB attacked the 5-fold symmetry axes as the *punched capsids* had dramatic dents on the capsid vertices. MxB might furthermore attack the portal cap, a cap of HSV1-pUL25 or its homologs in other herpesviruses, which seals the pUL6 portal after DNA packaging is completed (Liu *et al.*, 2019; McElwee *et al.*, 2018; Döhner et al. 2021; Naniima *et al.*, 2021). The high internal capsid pressure due to the negatively charged genome (Bauer *et al.*, 2013; Roos *et al.*, 2009) could support the MxB attack from the outside. The limited trypsin treatment might have primed the D capsids for disassembly, as they contained less pUL36, pUL17, pUL25, and pUL6 than the V capsids. However, MxB also attacked $V_{0.5}$ capsids that resemble cytosolic capsids during nuclear targeting or after nuclear egress (Ojala *et al.*, 2000; Wolfstein *et al.*, 2006; Radtke *et al.*, 2010; Anderson *et al.*, 2014); just not as fast, and not as efficient. Altogether, these results suggest that increasing tegumentation protects incoming and newly assembled capsids, possibly by masking the MxB target structure, or by inhibiting its GTPase cycle.

366 The MxB-mediated capsid disassembly required its NTE(1-25), GTP hydrolysis, and dimerization.
367 For the homologous MxA GTPase that limits infection of many RNA viruses (Haller *et al.*, 2015), Gao
368 *et al.* (2011) proposed a restriction mechanism that involves GTP hydrolysis and a mechano-chemical
369 coupling within ring-like oligomers with the GTPase domains being exposed on their outer diameter
370 (Gao *et al.*, 2011). Similarly, MxB can also assemble into helical tubes with the NTE and the GTPase
371 domain oriented outwards (Alvarez *et al.*, 2017). Accordingly, MxB monomers and dimers might
372 associate with the capsid vertices and insert between the hexons of neighbouring capsid faces. A
373 further oligomerization of MxB and/or conformational changes associated with GTP hydrolysis might
374 then exert destabilizing forces onto the capsid shells, and ultimately push the capsid faces apart.

375 **Does MxB induce capsid disassembly in cells?** Future studies need to investigate whether MxB
376 also induces the disassembly of herpesviral capsids in cells. Upon docking of an incoming capsid to a
377 NPC, the pUL25 portal cap is supposed to be displaced, the pUL6 portal to be opened, and the DNA
378 to be ejected from the capsid into the nucleoplasm due to this intramolecular repulsion (Brandariz-
379 Nunez *et al.*, 2019; Döhner *et al.*, 2021; Ojala *et al.*, 2000; Rode *et al.*, 2011). In uninfected cells, there
380 is a low amount of constitutively expressed MxB localized at the NPCs (Crameri *et al.*, 2018; Kane *et*
381 *al.*, 2018; Melen & Julkunen, 1997), which might dislodge the portal cap and open the capsid portal
382 on the incoming capsid to release the incoming genome into the nucleoplasm.

383 Crameri *et al.* (2018) proposed that the higher amounts of IFN-induced MxB may block cytosolic
384 capsid transport, genome uncoating at the NPCs, and/or the release of viral genomes into the
385 nucleoplasm, which is consistent with our biochemical data demonstrating MxB binding to HSV-1
386 capsids. MxB-mediated disassembly of capsids that we report here would further reduce capsid
387 targeting to the NPCs and genome release into the nucleoplasm. Accordingly, there are fewer HSV-1
388 capsid puncta in MxB expressing cells (Crameri *et al.*, 2018). Consistent with our data on capsid
389 disassembly with MxB(26-715), MxB(K131A), or MxB(M574D), restricting the infection of HSV-1,
390 MCMV, and MHV68 also requires the NTE, GTP hydrolysis, and dimerization of MxB (Crameri *et al.*,
391 2018; Schilling *et al.*, 2018). Restriction of HIV infection depends also on the NTE, to some extent on
392 the MxB GTPase function, and on its dimerization (Buffone *et al.*, 2015; Fricke *et al.*, 2014; Goujon *et*

al., 2014; Schulte *et al.*, 2015; Xie *et al.*, 2021). It will be interesting to determine whether MxB only competes for important HIV interactions with promoting host factors (reviewed in Temple *et al.*, 2020), or whether it also induces HIV capsid disassembly.

Our data together with Schilling *et al.* (2018) and Crameri *et al.* (2018) suggest that the IFN-inducible MxB restricts HSV-1, HSV-2, VZV, and possibly other herpesviruses, by promoting efficient capsid disassembly. We cannot exclude that a surplus of capsid- and NPC-associated MxB imposes further restrictions on intracellular transport and genome release into the nucleoplasm. However, if MxB(1-715) would disassemble viral capsids before they are oriented properly with their portal towards the NPCs, their genomes would end up in the cytosol and would not be delivered into the nucleoplasm. There are fewer incoming cytoplasmic capsids in cells expressing MxB (Crameri *et al.*, 2018), and incoming VP5 is ubiquitinated and degraded by proteasomes in macrophages (Horan *et al.*, 2013; Sun *et al.*, 2019). Therefore, capsid disassembly intermediates might be degraded in cells, while we could characterize them in our biochemical cell-free assays in which proteases had been blocked.

The viral genomes exposed after MxB-induced capsid disassembly might be degraded by the DNase TREX1 (Sun *et al.*, 2019), or stimulate the DNA sensors AIM2, cGAS, or IFI16, and the induction of antiviral host mechanisms. As an inoculation with destabilized HIV-1 capsids leads to an increased activation of the DNA sensor cGAS (Sumner *et al.*, 2020), the IFN-induced increased MxB expression might lead to a similar outcome in cells infected with herpesviruses. Accordingly, MxB may not only restrict herpesviruses by capsid disassembly, but also increase the exposure of viral genomes to cytosolic DNA sensors, which in turn would induce an IFN response, inflammation as well as innate and adaptive immune responses. Thus, MxB could be the long sought-after capsid sensor that destroys the sturdy herpesvirus capsids, and possibly HIV cores and other viral capsids, to promote host viral genome sensing.

MATERIALS AND METHODS

Cells. All cells were maintained in a humidified incubator at 37°C with 5% CO_2 and passaged twice per week. BHK-21 (ATCC CCL-10) and Vero cells (ATCC CCL-81) were cultured in MEM Eagle with 1% NEAA (Cytogen, Wetzlar, Germany) and 10% or 7.5% (v/v) FBS, respectively (Good Forte; PAN-Biotech, Aidenbach, Germany). THP-1 cells (ATCC TIB-202; kind gift from Walther Mothes, Yale University, New Haven, USA) were cultured in RPMI Medium 1640 (Thermo Fisher Scientific, Waltham, Massachusetts, United States) with 10% FBS (Thermo Fisher Scientific, Waltham, Massachusetts, United States). THP-1 were stimulated with 100 nM phorbol 12-myristate 13-acetate (PMA; Sigma-Aldrich, Germany) for 48 h and used immediately (Mϕ) or after 3 days of rest ($M\phi_R$). The cells were cultured with 1000 U/mL human type I IFN-α2a ($M\phi_{IFN}$; R&D Systems, Minneapolis, Minnesota, USA) or left untreated for 16 h.

A549 cells were cultured in DMEM with 10% FCS. In addition to A549 control cells, we used A549 cell lines stably expressing MxB(1-715), MxB(1-715/K131A), MxB(1-715/T151A), MxB(1-715/M574D), MxB(26-715), or MxA(1-662) upon transduction with the respective pLVX vectors with an engineered Kozak sequence to favor expression of the MxB(1-715) over the MxB(26-715) proteins (Schilling et al. 2018). Furthermore, we generated A549-MxBFLAG cells expressing MxB(1-715)FLAG and MxB(26-715)FLAG, both tagged with the FLAG epitope (GACTACAAAGACGATGACGACAAG) at the C-terminus of MxB (GenBAnk NM_002463), and A549-MxB(1-715)-MxB(26-715) cells expressing untagged MxB(1-715) and MxB(26-715) using the pLKOD-Ires-Puro vector (Clontech Takara Bio, Mountain View, United States). MeWo cells (kind gift from Graham Ogg; University of Oxford, Oxford, UK) were cultured in MEM with 10% FCS, NEAA, and 1 mM sodium pyruvate.

Viruses. Virus stocks of HSV-1(17^+)Lox (Sandbaumhüter *et al.*, 2013), HSV-1 strain KOS (Warner *et al.,* 1998; kind gift from Pat Spear, Northwestern Medical School, Chicago, USA), and HSV-2 strain 333 (Warner *et al.,* 1998; kind gift from Helena Browne, Cambridge University, Cambridge, UK) were prepared as reported before (Döhner *et al.*, 2006; Grosche *et al.*, 2019). Extracellular particles were harvested from the supernatant of BHK-21 cells infected with 3 to 4 x 10^4 PFU/mL (MOI of 0.01 PFU/cell) for 2 to 3 days until the cells had detached from the culture flasks, and plaque-titrated on Vero cells. VZV rOka (kind gift from Jeffrey Cohen, NIH, Bethesda, US) was maintained in infected

445 MeWo cells (Cohen & Seidel, 1993; Hertzog *et al.*, 2020). After 2 to 4 days, the VZV infected cells as
446 indicated by cytopathic effects were harvested, mixed with naïve MeWo cells at a ratio of 1:4 to 1:8
447 for continued culture. Aliquots of frozen infected cells were used to inoculate cultures used for
448 capsid preparation.

449 **HSV-1 infection.** THP-1 were seeded at 2.5 x 10^5 cells per 6-well, treated with 100 nM PMA
450 (Sigma-Aldrich, Germany) for 48 h and used immediately (Mϕ) or after 3 days of rest ($M\phi_R$). The cells
451 were then induced with 1000 U/mL of IFN-α ($M\phi_{IFN}$) or left untreated for 16 h. On the next day, they
452 were inoculated with HSV-1(17^+)Lox at 2.5 x 10^6, 2.5 x 10^7, or 5 x 10^7 PFU/mL (MOI of 5, 50, or 100
453 respectively) in CO_2-independent medium (Gibco Life Technologies) supplemented with 0.1% (w/v)
454 cell culture grade fatty-acid free bovine serum albumin (BSA; PAA Laboratories GmbH) for 30 min,
455 and then shifted to regular culture medium at 37°C and 5% CO_2. At the indicated times, the cells and
456 the corresponding media were harvested separately and snap-frozen in liquid nitrogen. These
457 samples as well as and HSV-1 and HSV-2 inocula were titrated on Vero cells (Döhner *et al.*, 2006;
458 Grosche *et al.*, 2019).

459 **Preparation of $V_{0.1}$, $V_{0.5}$ and V_1 and D capsids.** Extracellular HSV-1 or HSV-2 particles were
460 harvested by sedimentation at 12,000 rpm for 90 minutes at 4°C (Type 19 rotor, Beckman-Coulter)
461 from the medium of BHK-21 cells (40 x 175 cm² flasks; 2 – 2.5 x 10^7 cells/flask) infected with 0.01
462 PFU/cell (2 to 6.7 x 10^4 PFU/mL) for 2.5 days. The resulting medium pellets (MP) were resuspended in
463 2 mL of MKT buffer (20 mM MES, 30 mM Tris-HCl, 100 mM KCl, pH 7.4; Grosche et al., 2019; Radtke
464 et al., 2014; Turan et al., 2019), treated with 0.5 mg/mL trypsin (Sigma-Aldrich, Germany) at 37°C for
465 1 h which was then inactivated with 5 mg/mL trypsin inhibitor from soybean (SBTI; Fluka,
466 Switzerland) for 10 min on ice. These samples were then mixed with an equal volume of 2-fold lysis
467 buffer (2% TX-100, 20 mM MES, 30 mM Tris, pH 7.4, 20 mM DTT, 1x protease inhibitor cocktail [PIs,
468 Roche cOmplete] with 0.2 M, 1 M or 2 M KCl; Radtke et al., 2014). The samples were layered on top
469 of 20% (w/v) sucrose cushions in 20 mM MES, 30 mM Tris, pH 7.4 with 10 mM DTT, PIs with the
470 respective KCl concentration, and sedimented at 110,000 g for 20 min at 4°C (TLA-120.2 rotor,
471 Beckman-Coulter). The supernatants and the cushions containing solubilized viral envelope and

tegument proteins were carefully removed. The pellets were resuspended in BRB80 (80 mM PIPES, pH 6.8, 12 mM $MgCl_2$, 1 mM EGTA) with 10 mM DTT, PIs, 0.1 U/mL protease-free DNase I (Promega, USA), and 100 mg/mL protease-free RNase (Roth GmbH, Germany) for 1 h at 37°C and then overnight at 4°C. The capsids were sedimented at 110,000 g for 15 min at 4°C (TLA-120.2) and resuspended in capsid binding buffer (CBB: 5% [w/v] sucrose, 20 mM HEPES-KOH, pH 7.3, 80 mM K-acetate, 1 mM EGTA, 2 mM Mg-acetate, 10 mM DTT and PIs) by ultrasound tip sonication at 40 W for about 5 x 5 seconds on ice. Furthermore, we treated $V_{0.1}$ capsids for 40 min at 37°C with 10 µg/mL trypsin in CBB lacking PIs to generate D capsids by limited digestion. After the addition of 5 mg/mL SBTI for 10 min on ice to block the trypsin activity, the D capsids were sedimented at 110,000 x g and 4°C for 15 min (TLA-120.2), and resuspended in CBB with PIs.

Preparation of nuclear A, B, and C capsids. HSV-1 nuclear capsids were prepared from 40 x 175 cm^2 flasks with BHK-21 cells infected with 0.01 PFU/cell (3 to 4 x 10^4 PFU/mL) for about 2.5 days (Anderson *et al.*, 2014; Radtke *et al.*, 2010; Radtke *et al.*, 2014; Snijder *et al.*, 2017; Wolfstein *et al.*, 2006). VZV nuclear capsids were harvested from infected MeWo cells cultured in 5 to 10 x 175 cm^2 flasks at maximum syncytia formation but before cell lysis. The cells were harvested, resuspended in MKT buffer (20 mM MES, 30 mM Tris, pH 7.4, 100 mM KCl), snap-frozen, and stored at -80°C. Nuclear A, B, and C capsids were separated by sedimentation at 50,000 x g and 4°C for 80 min (SW40Ti, Beckman Coulter) on linear 20 to 50% sucrose gradients in TKE buffer (20 mM Tris, pH 7.5, 500 mM KCl, 1 mM EDTA; diluted in three volumes of TKE supplemented with 2 mM DTT and PIs (Roche cOmplete). The capsids were sedimented in BSA-coated centrifuge tubes at 110,000 g at 4°C for 20 min (TLA-120.2), resuspended in BRB80 buffer supplemented with 100 mg/mL RNase (Roth, Germany), 0.1 U/mL DNase I (M6101, Promega, USA), 10 mM DTT, and PIs, sedimented again, and resuspended in CBB with PIs.

Calibration of capsid concentration. To calibrate the amount of capsid equivalents (CAP_{eq}) among different experiments, we compared all capsid preparations used in this study with a calibration curve generated from the same starting preparation. The capsids were suspended in sample buffer (1% [w/v] SDS, 50 mM Tris-HCl, pH 6.8, 1% [v/v] β-mercaptoethanol, 5% [v/v] glycerol,

PIs [Roche cOmplete]), and adsorbed to nitrocellulose membranes (BioTrace™, Pall Laboratory) using a 48-slot suction device (Bio-DOT-SF, Bio-Rad, Hercules, California, USA). The membranes were probed with a polyclonal rabbit serum raised against purified HSV-1 nuclear capsids (SY4563; Table S4; Döhner *et al.,* 2018) followed by secondary antibodies conjugated to fluorescent infrared dyes (donkey-anti-rabbit IgG-IRDye1 800CW; Table S3), and documented with an Infrared Imaging System (Odyssey, Image Studio Lite Quantification Software, LI-COR Biosciences, Lincoln, Nebraska, USA). MPs harvested from one 175 cm² flasks of BHK-21 cells infected with HSV-1 contained about 0.5 to 1 x 10^9 PFU/mL, and 0.75 to 1.5 x 10^9 CAP_{eq}/mL. A nuclear HSV-1 capsid fraction prepared from one 175 cm² flask contained about 0.5 to 1 x 10^7 CAP_{eq} of A capsids, 1 to 2 x 10^7 CAP_{eq} of B capsids, and 0.5 to 0.75 x 10^7 CAP_{eq} of C capsids, and a nuclear VZV fraction from one 175 cm² flasks of MeWo cells 2 to 4 x 10^5 CAP_{eq} of A capsids, 0.5 to 1 x 10^6 CAP_{eq} of B capsids, and 0.8 to 1.6 x 10^7 CAP_{eq} of C capsids. Capsid-host protein complexes were assembled *in-solution* using 7.5 x 10^8 CAP_{eq}/condition for MS and immunoblot experiments, and for the *on-grid* electron microscopy assay 2 x 10^7 CAP_{eq}/condition were used.

Preparation of cytosol. Cytosolic extracts were prepared as described before (Radtke *et al.*, 2010; Radtke *et al.*, 2014), dialyzed (7K MW cut-off cassettes; Slide-A-Lyzer™, Thermo Scientific), snap-frozen and stored at -80°C. Prior to their use, the cytosols were supplemented with 1 mM ATP, 1 mM GTP, 7 mM creatine phosphate, 5 mM DTT, and PIs (Roche cOmplete), and centrifuged at 130,000 g for 30 min at 4°C (TLA-120.2). We added nocodazole to 25 µM to the cytosols, and left them either untreated (ATP/GTP^{high}) or supplemented them with 10 U/mL apyrase (Sigma; ATP/GTP^{low}) for 15 min at RT.

Assembly of capsid-host protein complexes *in-solution*. Capsids were resuspended in CBB and cytosol at a protein concentration of 0.2 mg/mL in an assay volume of 60 µL per sample on a rotating platform at 800 rpm for 1 h at 37°C (c.f. Fig. S1). The capsid-host protein complexes were sedimented through a 30% sucrose cushion at 110,000 g for 20 min at 4°C (TLA-100, Beckman-Coulter), resuspended in CBB by ultrasound tip sonication at 40 W for about 5 x 5 seconds on ice, and analysed by mass spectrometry, immunoblot, or electron microscopy (Radtke *et al.*, 2014).

SDS-PAGE and immunoblot. The samples were lysed in Laemmli buffer (1% [w/v] SDS, 50 mM Tris-HCl, pH 6.8, 1% [v/v] β-mercaptoethanol, 5% [v/v] glycerol, bromophenol blue, PIs [Roche cOmplete]). The proteins were separated on linear 7.5 to 12% or 10 to 15% SDS-PAGE, transferred to methanol-activated PVDF membranes, probed with rabbit or murine primary antibodies (Table S3) and secondary antibodies conjugated to fluorescent infrared dyes (anti-rabbit IgG-IRDye1 800CW; anti-mouse IgG-IRDye1 680RD; Table S3) and documented with an Infrared Imaging System (Odyssey, Image Studio Lite Quantification Software, LI-COR Biosciences, Lincoln, Nebraska, USA).

Mass spectrometry sample preparation and measurement. Capsid-host protein complexes were analysed by liquid chromatography coupled to tandem mass spectrometry (LC-MS/MS) in four independent biological replicates. The samples were resuspended in hot Laemmli buffer and separated in NuPAGE™ 4 to 12% Bis-Tris protein gels (Invitrogen) before *in*-gel digestion. Briefly, proteins were fixed and stained by Coomassie solution (0.4% G250, 30% methanol, 10% acetic acid). Sample lanes were excised, destained (50% ethanol, 25 mM ammonium bi-carbonate), dehydrated with 100% ethanol and dried using a SpeedVac centrifuge (Eppendorf, Concentrator plus). Gel pieces were rehydrated in trypsin solution (1/50 [w/w] trypsin/protein) overnight at 37°C. Tryptic peptides were extracted in extraction buffer (3% trifluoroacetic acid, 30% acetonitrile), dried using a SpeedVac centrifuge, resuspended in 2 M Tris-HCl buffer before reduction and alkylation using 10 mM Tris(2-carboxyethyl)phosphine, 40 mM 2-Chloroacetamide in 25 mM Tris-HCl pH 8.5. The peptides were purified, concentrated on StageTips with three C18 Empore filter discs (3M), separated on a liquid chromatography instrument, and analysed by mass spectrometry (EASY- nLC 1200 system on an LTQ-Orbitrap XL; Thermo Fisher Scientific) as described before (Hubel *et al.*, 2019). Peptides were loaded on a 20 cm reverse-phase analytical column (75 µm column diameter; ReproSil-Pur C18-AQ 1.9 µm resin; Dr. Maisch) and separated using a 120 min acetonitrile gradient. The mass spectrometer was operated in Data-Dependent Analysis mode (DDA, XCalibur software v.3.0, Thermo Fisher).

Mass-spectrometry data analysis. Raw files were processed with MaxQuant using iBAQ quantification and Match Between Runs option, and the protein groups were filtered with Perseus for reverse identification, modification site only identification, and MaxQuant contaminant list

(https://maxquant.net/maxquant/, v1.6.2.10; https://maxquant.net/perseus/, v1.6.5.0; Cox & Mann, 2008; Tyanova *et al.*, 2016a; Tyanova *et al.*, 2016b). The iBAQ intensities were normalized across all samples to the overall median intensity of the HSV-1 capsid protein VP5. Cytosol and beads incubated with cytosol samples were normalized to all proteins detected in at least three replicates in each condition. Significant differences between given conditions were determined by a two-sided Welch t-test on protein groups present in three replicates of at least one condition, followed by permutation-based FDR statistics (250 permutations), using an absolute $\log_2$ difference cut-off of 1.5 and an FDR cut-off of 0.01. To characterize the IFN induction, we annotated proteins reported as being induced by IFN type-I as *ISGs* proteins (InterferomeDB, > 2x change; http://www.interferome.org/interferome/home.jspx; Rusinova *et al.*, 2013). We used the Fisher'3 exact test against *ISGs* proteins as well as all Gene Ontology (GO) terms for enrichment analysis of proteins upregulated in IFN-induced $M\phi_{IFN}$ cytosol over $M\phi_R$ cytosol ($\log_2$ difference ≥ 1.5; unadjusted p-value < 0.05). The data were summarized in volcano or bar plots (GraphPad Prism v5.0, https://www.graphpad.com/; Perseus v1.6.5.0; Tyanova *et al.*, 2016b).

Interaction Network Assembly. We focused our analysis on proteins that showed specific differences from one capsid preparation to the other, within the same cytosol preparation, and considered host proteins with an enrichment higher than 1.5 $\log_2$ fold changes and a permutation-based FDR < 0.05 as specifically enriched. To visualize enrichment among different capsid-host protein complexes, we generated integrative networks using Cytoscape (http://www.cytoscape.org/; v3.7.2) and STRING (confidence score: 0.7; Szklarczyk *et al.*, 2019). STRING uses a combination of databases on co-expression, conserved occurrences, GO terms and Kyoto Encyclopedia of Genes and Genomes (KEGG; https://www.genome.jp/kegg/; Kanehisa & Goto, 2000; Kanehisa, 2019; Kanehisa *et al.*, 2021). To assemble pathway enrichments, we used DAVID, a Database for Annotation, Visualization and Integrated Discovery (https://david.ncifcrf.gov/home.jsp; v6.8; Huang da *et al.*, 2009a; Huang da *et al.*, 2009b) and the Cytoscape plug-ins ClueGO and CluePedia (http://apps.cytoscape.org/apps/cluego, v2.5.7; http://apps.cytoscape.org/apps/cluepedia, v1.5.7; Bindea *et al.*, 2009; Bindea *et al.*, 2013).

Electron microscopy. Capsid-host protein complexes were assembled at ATP/GTP^{high} in solution, harvested by ultracentrifugation, resuspended in CBB, and adsorbed onto enhanced hydrophilicity-400 mesh formvar- and carbon-coated copper grids (Stork Veco, The Netherlands; Radtke *et al.*, 2010; Roos *et al.*, 2009). Moreover, capsids at a concentration of 1 x 10^7 CAP_{eq}/mL were adsorbed directly for 20 min at RT onto the grids. The grids were incubated on a 10 µL drop of cytosol with a protein concentration of 0.2 mg/mL and ATP/GTP^{high} in a humid chamber for 1 h at 37°C. The samples were left untreated or labelled with anti-VP5 (pAb NC-1) and protein-A gold (10 nm diameter; Cell Microscopy Centre, Utrecht School of Medicine, The Netherlands). For both protocols, the grids were washed with PBS and ddH_2O, contrasted with 2% uranyl acetate at pH 4.4, air dried, and analysed by transmission electron microscopy (Morgani or Tecnai; FEI, Einthoven, The Netherlands). The capsid morphology was evaluated for about 100 structures/assay from about 15 randomly selected images of 2.7 µm² of three biological replicates. We classified capsomer-containing structures as *punched*, if they lacked one or more of their vertices but still had an icosahedral shape, and as *flat shells*, if they lacked the icosahedral shape but contained capsomers, and scored them as one capsid equivalent structure if they contained more than 100 capsomers.

Capsid DNA uncoating assay. D capsids were incubated with cytosols from A549-control, A549-MxB(1-715), A549-MxB(M574D), or A549-MxB-FLAG for 1 h at 37°C or treated for 5 min with 1% SDS followed by 10 min with 10% TX-100(Ojala *et al.*, 2000). The viral genomes released during the assay were degraded by adding 50 U/mL of benzonase for 1 h at 37°C, and the remaining protected DNA was purified with the DNA Blood Mini Kit (Qiagen, Hilden, Germany) and quantified by real-time PCR on a qTower^3 (Analytik Jena, Jena, Germany). The SYBR Green assay was performed with the Luna Universal qPCR Master Mix (NEB, Ipswich, MA, USA) according to the manufacturer's instructions with primers specific for HSV-1 gB (UL27 gene) (HSV1_2 SYBR fwd: 5'-gtagccgtaaaacggggaca-3' and HSV1_2 SYBR rev: 5'-ccgacctcaagtacaacccc-3'; Engelmann *et al.*, 2008). Standards and samples were run in triplicates and results expressed as % released viral DNA with the SDS/Tx-100 treatment normalized to 100%.

606 **Quantification and statistical analyses.** We performed Welch's t-testing, Kruskal-Wallis H-testing,
607 Friedman and one-way analyses of variance with a Dunns or Bonferroni post-testing (GraphPad Prism
608 v5.0; https://www.graphpad.com/).

609 **Data availability:** The datasets produced in this study are available at PRIDE (PXD028276;
610 http://www.ebi.ac.uk/pride). The published article will include all datasets generated and analysed.

611 ACKNOWLEDGMENT

612 We thank Katinka Döhner and Franziska Hüsers (Institute of Virology, Hannover Medical School)
613 as well as Miriam Schilling (University of Oxford, UK) for many constructive discussions and feedback
614 on the manuscript, and Jasper Götting (Institute of Virology, Hannover Medical School) for support
615 on bioinformatics analyses. We are grateful to Ari Helenius (ETH Zürich, Switzerland), Graham Ogg
616 (University of Oxford, UK), Gary Cohen (University of Pennsylvania, USA),Helena Browne (Cambridge
617 University, UK), Jay Brown (University of Virginia, USA), Jeffrey Cohen (NIH, Bethesda, USA), Pat
618 Spear (Northwestern Medical School, USA), and Roselyn Eisenberg (University of Pennsylvania, USA)
619 for their generous donation of virus strains and invaluable antibodies.

620 Our research was supported by the EU 7th framework (Marie-Curie Actions ITN-EDGE;
621 https://ec.europa.eu/research/mariecurieactions/about/innovative-training-networks_en, H2020-EU.1.3.1,
622 #675278 to JR, AP, and BS), the UK MRC (core funding of theMedical Research Council Human
623 Immunology Unit to JR), the NIH (NIGMS, GM114141 to IMC), an EU ERC consolidator grant (ERC-CoG
624 ProDAP 817798 to AP), and the German Research Foundation (http://www.dfg.de/; PI1084/3,
625 PI1084/4, PI1084/5, TRR179, and TRR237 to AP; KO1579/13 to GK; CRC900 C2 158989968, EXC62
626 REBIRTH 24102914, EXC2155 RESIST 390874280, SO403/6 to BS). The funders had no role in study
627 design, data collection and analysis, decision to publish, or preparation of the manuscript.

628 AUTHOR CONTRIBUTIONS

629 MCS and BS conceived and wrote the article. MCS, VG, APir, AHM, TG, FA, IC, APic, and BS
630 contributed to the development of methodology. MCS, VG, SW, and ARN performed experiments

631 and curated the respective data. MCS, VG, APir, APic, and BS analysed the data. MCS, AHM, JH, AB,
632 APo, UP, and SW produced the resources used in this study. FA, SW, TG, RB, IC, JR, and GK
633 contributed to the analysis of the data and the discussion of the content. All authors reviewed and
634 edited the manuscript before submission.

635 ## COMPETING INTEREST

636 The authors have declared that no competing interests exist.

637 # REFERENCES

638 Alvarez FJD, He S, Perilla JR, Jang S, Schulten K, Engelman AN, Scheres SHW, & Zhang P (2017)
639 CryoEM structure of MxB reveals a novel oligomerization interface critical for HIV restriction. *Sci*
640 *Adv* **3**: e1701264

641 Anderson F, Savulescu AF, Rudolph K, Schipke J, Cohen I, Ibiricu I, Rotem A, Grunewald K, Sodeik B, &
642 Harel A (2014) Targeting of viral capsids to nuclear pores in a cell-free reconstitution system.
643 *Traffic* **15**: 1266-1281

644 Arvin AM & Abendroth A (2021) Varicella–Zoster Virus. In *Fields Virology: DNA Viruses,* Howley PM,
645 Knipe DM, Cohen JL, Damania BA (eds) pp 445-488. Wolters Kluwer Health/Lippincott Williams &
646 Wilkins; 7th edition (May 17, 2021): Berlin, Heidelberg

647 Ashburner M, Ball CA, Blake JA, Botstein D, Butler H, Cherry JM, Davis AP, Dolinski K, Dwight SS, Eppig
648 JT, Harris MA, Hill DP, Issel-Tarver L, Kasarskis A, Lewis S, Matese JC, Richardson JE, Ringwald M,
649 Rubin GM, & Sherlock G (2000) Gene ontology: tool for the unification of biology. The Gene
650 Ontology Consortium. *Nat Genet* **25**: 25-29

651 Bauer DW, Huffman JB, Homa FL, & Evilevitch A (2013) Herpes virus genome, the pressure is on. *J Am*
652 *Chem Soc* **135**: 11216-11221

653 Betancor G, Dicks MDJ, Jimenez-Guardeño JM, Ali NH, Apolonia L, & Malim MH (2019) The GTPase
654 Domain of MX2 Interacts with the HIV-1 Capsid, Enabling Its Short Isoform to Moderate Antiviral
655 Restriction. *Cell Rep* **29**: 1923-1933.e3

656 Bindea G, Galon J, & Mlecnik B (2013) CluePedia Cytoscape plugin: pathway insights using integrated
657 experimental and in silico data. *Bioinformatics* **29**: 661-663

658 Bindea G, Mlecnik B, Hackl H, Charoentong P, Tosolini M, Kirilovsky A, Fridman WH, Pages F,
659 Trajanoski Z, & Galon J (2009) ClueGO: a Cytoscape plug-in to decipher functionally grouped gene
660 ontology and pathway annotation networks. *Bioinformatics* **25**: 1091-1093

661 Brandariz-Nunez A, Liu T, Du T, & Evilevitch A (2019) Pressure-driven release of viral genome into a
662 host nucleus is a mechanism leading to herpes infection. *Elife* **8**: 10.7554/eLife.47212

663 Buffone C, Schulte B, Opp S, & Diaz-Griffero F (2015) Contribution of MxB oligomerization to HIV-1
664 capsid binding and restriction. *J Virol* **89**: 3285-3294

665 Cabrera JR, Manivanh R, North BJ, & Leib DA (2019) The ESCRT-Related ATPase Vps4 Is Modulated by
666 Interferon during Herpes Simplex Virus 1 Infection. *mBio* **10**: 10.1128/mBio.02567-18

667 Cao H, Krueger EW, Chen J, Drizyte-Miller K, Schulz ME, & McNiven MA (2020) The anti-viral dynamin
668 family member MxB participates in mitochondrial integrity. *Nat Commun* **11**: 1048-w

669 Carter-Timofte ME, Paludan SR, & Mogensen TH (2018) RNA Polymerase III as a Gatekeeper to
670 Prevent Severe VZV Infections. *Trends Mol Med* **24**: 904-915

671 Chen Y, Zhang L, Graf L, Yu B, Liu Y, Kochs G, Zhao Y, & Gao S (2017) Conformational dynamics of
672 dynamin-like MxA revealed by single-molecule FRET. *Nat Commun* **8**: 15744

673 Cohen GH, Ponce de Leon M, Diggelmann H, Lawrence WC, Vernon SK, & Eisenberg RJ (1980)
674 Structural analysis of the capsid polypeptides of herpes simplex virus types 1 and 2. *J Virol* **34**:
675 521-531

676 Cohen JI & Seidel KE (1993) Generation of varicella-zoster virus (VZV) and viral mutants from cosmid
677 DNAs: VZV thymidylate synthetase is not essential for replication in vitro. *Proc Natl Acad Sci U S A*
678 **90**: 7376-7380

679 Coller KE, Lee JI, Ueda A, & Smith GA (2007) The capsid and tegument of the alphaherpesviruses are
680 linked by an interaction between the UL25 and VP1/2 proteins. *J Virol* **81**: 11790-11797

681 Cox J & Mann M (2008) MaxQuant enables high peptide identification rates, individualized p.p.b.-
682 range mass accuracies and proteome-wide protein quantification. *Nat Biotechnol* **26**: 1367-1372

683 Crameri M, Bauer M, Caduff N, Walker R, Steiner F, Franzoso FD, Gujer C, Boucke K, Kucera T,
684 Zbinden A, Munz C, Fraefel C, Greber UF, & Pavlovic J (2018) MxB is an interferon-induced
685 restriction factor of human herpesviruses. *Nat Commun* **9**: 1980-2

686 Crump CM (2018) Virus Assembly and Egress of HSV. *Adv Exp Med Biol* **1045**: 23-44

687 Crump CM, Yates C, & Minson T (2007) Herpes simplex virus type 1 cytoplasmic envelopment
688 requires functional Vps4. *J Virol* **81**: 7380-7387

689 Dai X & Zhou ZH (2018) Structure of the herpes simplex virus 1 capsid with associated tegument
690 protein complexes. *Science* **360**: 10.1126/science.aao7298. Epub 2018 Apr 5

691 Diefenbach RJ (2015) Conserved tegument protein complexes: Essential components in the assembly
692 of herpesviruses. *Virus Res* **210**: 308-317

693 Döhner K, Cornelius A, Serrero MC, & Sodeik B (2021) Herpesvirus Capsids on Their Journey to the
694 Center of the Cell. *Current Opinion of Virology* **50**: 147-158

695 Döhner K, Ramos-Nascimento A, Bialy D, Anderson F, Hickford-Martinez A, Rother F, Koithan T,
696 Rudolph K, Buch A, Prank U, Binz A, Hugel S, Lebbink RJ, Hoeben RC, Hartmann E, Bader M,
697 Bauerfeind R, & Sodeik B (2018) Importin alpha1 is required for nuclear import of herpes simplex
698 virus proteins and capsid assembly in fibroblasts and neurons. *PLoS Pathog* **14**: e1006823

699 Döhner K, Radtke K, Schmidt S, & Sodeik B (2006) Eclipse phase of herpes simplex virus type 1
700 infection: Efficient dynein-mediated capsid transport without the small capsid protein VP26. *J*
701 *Virol* **80**: 8211-8224

702 Engelmann I, Petzold DR, Kosinska A, Hepkema BG, Schulz TF, & Heim A (2008) Rapid quantitative
703 PCR assays for the simultaneous detection of herpes simplex virus, varicella zoster virus,
704 cytomegalovirus, Epstein-Barr virus, and human herpesvirus 6 DNA in blood and other clinical
705 specimens. *J Med Virol* **80**: 467-477

706 Everett RD, Meredith M, Orr A, Cross A, Kathoria M, & Parkinson J (1997) A novel ubiquitin-specific
707 protease is dynamically associated with the PML nuclear domain and binds to a herpesvirus
708 regulatory protein. *EMBO J* **16**: 1519-1530

709 Flohr F, Schneider-Schaulies S, Haller O, & Kochs G (1999) The central interactive region of human
710 MxA GTPase is involved in GTPase activation and interaction with viral target structures. *FEBS Lett*
711 **463**: 24-28

712 Fribourgh JL, Nguyen HC, Matreyek KA, Alvarez FJD, Summers BJ, Dewdney TG, Aiken C, Zhang P,
713 Engelman A, & Xiong Y (2014) Structural insight into HIV-1 restriction by MxB. *Cell Host Microbe*
714 **16**: 627-638

715 Fricke T, White TE, Schulte B, de Souza Aranha Vieira, D. A., Dharan A, Campbell EM, Brandariz-Nunez
716 A, & Diaz-Griffero F (2014) MxB binds to the HIV-1 core and prevents the uncoating process of
717 HIV-1. *Retrovirology* **11**: 68-x

718 Gao S, von der Malsburg A, Dick A, Faelber K, Schroder GF, Haller O, Kochs G, & Daumke O (2011)
719 Structure of myxovirus resistance protein a reveals intra- and intermolecular domain interactions
720 required for the antiviral function. *Immunity* **35**: 514-525

721 Gene Ontology Consortium (2021) The Gene Ontology resource: enriching a GOld mine. *Nucleic Acids*
722 *Res* **49**: D325-D334

723 Gershon AA, Breuer J, Cohen JI, Cohrs RJ, Gershon MD, Gilden D, Grose C, Hambleton S, Kennedy PG,
724 Oxman MN, Seward JF, & Yamanishi K (2015) Varicella zoster virus infection. *Nat Rev Dis Primers*
725 **1**: 15016

726 Goujon C, Moncorge O, Bauby H, Doyle T, Barclay WS, & Malim MH (2014) Transfer of the amino-
727 terminal nuclear envelope targeting domain of human MX2 converts MX1 into an HIV-1 resistance
728 factor. *J Virol* **88**: 9017-9026

729 Goujon C, Moncorge O, Bauby H, Doyle T, Ward CC, Schaller T, Hue S, Barclay WS, Schulz R, & Malim
730 MH (2013) Human MX2 is an interferon-induced post-entry inhibitor of HIV-1 infection. *Nature*
731 **502**: 559-562

Grosche L, Döhner K, Düthorn A, Hickford-Martinez A, Steinkasserer A, & Sodeik B (2019) Herpes Simplex Virus Type 1 Propagation, Titration and Single-step Growth Curves. *Bio-protocol*: e3441

Haller O, Staeheli P, Schwemmle M, & Kochs G (2015) Mx GTPases: dynamin-like antiviral machines of innate immunity. *Trends Microbiol* **23**: 154-163

Hammond C & Helenius A (1994) Quality control in the secretory pathway: retention of a misfolded viral membrane glycoprotein involves cycling between the ER, intermediate compartment, and Golgi apparatus. *J Cell Biol* **126**: 41-52

Hertzog J, Rigby RE, Roll S, Cursi C, Chauveau L, Davenne T, & Rehwinkel J (2021) Varicella-Zoster Virus ORF9 Is an Antagonist of the DNA Sensor cGAS. *bioRxiv*: 2020.02.11.943415v2

Hertzog J & Rehwinkel J (2020) Regulation and inhibition of the DNA sensor cGAS. *EMBO Rep* **21**: e51345

Horan KA, Hansen K, Jakobsen MR, Holm CK, Soby S, Unterholzner L, Thompson M, West JA, Iversen MB, Rasmussen SB, Ellermann-Eriksen S, Kurt-Jones E, Landolfo S, Damania B, Melchjorsen J, Bowie AG, Fitzgerald KA, & Paludan SR (2013) Proteasomal degradation of herpes simplex virus capsids in macrophages releases DNA to the cytosol for recognition by DNA sensors. *J Immunol* **190**: 2311-2319

Huang da W, Sherman BT, & Lempicki RA (2009a) Bioinformatics enrichment tools: paths toward the comprehensive functional analysis of large gene lists. *Nucleic Acids Res* **37**: 1-13

Huang da W, Sherman BT, & Lempicki RA (2009b) Systematic and integrative analysis of large gene lists using DAVID bioinformatics resources. *Nat Protoc* **4**: 44-57

Hubel P, Urban C, Bergant V, Schneider WM, Knauer B, Stukalov A, Scaturro P, Mann A, Brunotte L, Hoffmann HH, Schoggins JW, Schwemmle M, Mann M, Rice CM, & Pichlmair A (2019) A protein-interaction network of interferon-stimulated genes extends the innate immune system landscape. *Nat Immunol* **20**: 493-502

Huet A, Makhov AM, Huffman J, Vos M, Homa FL, & Conway JF (2016) Extensive subunit contacts underpin herpesvirus capsid stability and interior-to-exterior allostery. *Nat Struc & Mol Biol* **23**: 531-540

Huffmaster NJ, Sollars PJ, Richards AL, Pickard GE, & Smith GA (2015) Dynamic ubiquitination drives herpesvirus neuroinvasion. *Proc Natl Acad Sci U S A* **112**: 12818-12823

Justice JL, Kennedy MA, Hutton JE, Liu D, Song B, Phelan B, & Cristea IM (2021) Systematic profiling of protein complex dynamics reveals DNA-PK phosphorylation of IFI16 en route to herpesvirus immunity. *Sci Adv* **7**: 10.1126/sciadv.abg6680. Print 2021 Jun

Kane M, Yadav SS, Bitzegeio J, Kutluay SB, Zang T, Wilson SJ, Schoggins JW, Rice CM, Yamashita M, Hatziioannou T, & Bieniasz PD (2013) MX2 is an interferon-induced inhibitor of HIV-1 infection. *Nature* **502**: 563-566

Kane M, Rebensburg SV, Takata MA, Zang TM, Yamashita M, Kvaratskhelia M, & Bieniasz PD (2018) Nuclear pore heterogeneity influences HIV-1 infection and the antiviral activity of MX2. *Elife* **7**: 10.7554/eLife.35738

Kanehisa M (2019) Toward understanding the origin and evolution of cellular organisms. *Protein Sci* **28**: 1947-1951

Kanehisa M, Furumichi M, Sato Y, Ishiguro-Watanabe M, & Tanabe M (2021) KEGG: integrating viruses and cellular organisms. *Nucleic Acids Res* **49**: D545-D551

Kanehisa M & Goto S (2000) KEGG: kyoto encyclopedia of genes and genomes. *Nucleic Acids Res* **28**: 27-30

King MC, Raposo G, & Lemmon MA (2004) Inhibition of nuclear import and cell-cycle progression by mutated forms of the dynamin-like GTPase MxB. *Proc Natl Acad Sci U S A* **101**: 8957-8962

Knipe DM, Heldwein EE, Mohr IJ, Sodroski CN (2021) Herpes Simplex Viruses: Mechanisms of Lytic and Latent Infection. In *Fields Virology: DNA Viruses,* Howley PM, Knipe DM, Cohen JL, Damania

780 BA (eds) pp 235-296. Wolters Kluwer Health/Lippincott Williams & Wilkins; 7th edition (May 17,
781 2021)

782 Kurt-Jones EA, Orzalli MH, & Knipe DM (2017) Innate Immune Mechanisms and Herpes Simplex Virus
783 Infection and Disease. *Adv Anat Embryol Cell Biol* **223**: 49-75

784 Liu SY, Sanchez DJ, Aliyari R, Lu S, & Cheng G (2012) Systematic identification of type I and type II
785 interferon-induced antiviral factors. *Proc Natl Acad Sci U S A* **109**: 4239-4244

786 Liu YT, Jih J, Dai X, Bi GQ, & Zhou ZH (2019) Cryo-EM structures of herpes simplex virus type 1 portal
787 vertex and packaged genome. *Nature* **570**: 257-261

788 Liu Z, Pan Q, Ding S, Qian J, Xu F, Zhou J, Cen S, Guo F, & Liang C (2013) The interferon-inducible MxB
789 protein inhibits HIV-1 infection. *Cell Host Microbe* **14**: 398-410

790 Lum KK & Cristea IM (2021) Host Innate Immune Response and Viral Immune Evasion During
791 Alphaherpesvirus Infection. *Curr Issues Mol Biol* **42**: 635-686

792 Ma Z, Ni G, & Damania B (2018) Innate Sensing of DNA Virus Genomes. *Annu Rev Virol* **5**: 341-362

793 McElwee M, Vijayakrishnan S, Rixon F, & Bhella D (2018) Structure of the herpes simplex virus portal-
794 vertex. *PLoS Biol* **16**: e2006191

795 Melen K & Julkunen I (1997) Nuclear cotransport mechanism of cytoplasmic human MxB protein. *J*
796 *Biol Chem* **272**: 32353-32359

797 Melen K, Keskinen P, Ronni T, Sareneva T, Lounatmaa K, & Julkunen I (1996) Human MxB protein, an
798 interferon-alpha-inducible GTPase, contains a nuclear targeting signal and is localized in the
799 heterochromatin region beneath the nuclear envelope. *J Biol Chem* **271**: 23478-23486

800 Naniima P, Naimo E, Koch S, Curth U, Alkharsah KR, Stroh LJ, Binz A, Beneke JM, Vollmer B, Boning H,
801 Borst EM, Desai P, Bohne J, Messerle M, Bauerfeind R, Legrand P, Sodeik B, Schulz TF, & Krey T
802 (2021) Assembly of infectious Kaposi's sarcoma-associated herpesvirus progeny requires
803 formation of a pORF19 pentamer. *PLoS Biol* **19**: e3001423

804 Newcomb WW & Brown JC (1991) Structure of the herpes simplex virus capsid: effects of extraction
805 with guanidine hydrochloride and partial reconstitution of extracted capsids. *J Virol* **65**: 613-620

806 Ojala PM, Sodeik B, Ebersold MW, Kutay U, & Helenius A (2000) Herpes simplex virus type 1 entry
807 into host cells: reconstitution of capsid binding and uncoating at the nuclear pore complex in
808 vitro. *Mol Cell Biol* **20**: 4922-4931

809 Page HG & Read GS (2010) The virion host shutoff endonuclease (UL41) of herpes simplex virus
810 interacts with the cellular cap-binding complex eIF4F. *J Virol* **84**: 6886-6890

811 Paludan SR, Reinert LS, & Hornung V (2019) DNA-stimulated cell death: implications for host defence,
812 inflammatory diseases and cancer. *Nat Rev Immunol* **19**: 141-153

813 Pilla C, Emanuelli T, Frassetto SS, Battastini AM, Dias RD, & Sarkis JJ (1996) ATP diphosphohydrolase
814 activity (apyrase, EC 3.6.1.5) in human blood platelets. *Platelets* **7**: 225-230

815 Radtke K, Anderson F, & Sodeik B (2014) A precipitation-based assay to analyze interactions of viral
816 particles with cytosolic host factors. *Methods Mol Biol* **1144**: 191-208

817 Radtke K, Kieneke D, Wolfstein A, Michael K, Steffen W, Scholz T, Karger A, & Sodeik B (2010) Plus-
818 and minus-end directed microtubule motors bind simultaneously to herpes simplex virus capsids
819 using different inner tegument structures. *PLoS Pathog* **6**: e1000991

820 Rode K, Döhner K, Binz A, Glass M, Strive T, Bauerfeind R, & Sodeik B (2011) Uncoupling uncoating of
821 herpes simplex virus genomes from their nuclear import and gene expression. *J Virol* **85**: 4271-
822 4283

823 Rodriguez MC, Dybas JM, Hughes J, Weitzman MD, & Boutell C (2020) The HSV-1 ubiquitin ligase
824 ICP0: Modifying the cellular proteome to promote infection. *Virus Res* **285**: 198015

825 Roos WH, Radtke K, Kniesmeijer E, Geertsema H, Sodeik B, & Wuite GJ (2009) Scaffold expulsion and
826 genome packaging trigger stabilization of herpes simplex virus capsids. *Proc Natl Acad Sci U S A*
827 **106**: 9673-9678

Rusinova I, Forster S, Yu S, Kannan A, Masse M, Cumming H, Chapman R, & Hertzog PJ (2013) Interferome v2.0: an updated database of annotated interferon-regulated genes. *Nucleic Acids Res* **41**: 1040

Sae-Ueng U, Liu T, Catalano CE, Huffman JB, Homa FL, & Evilevitch A (2014) Major capsid reinforcement by a minor protein in herpesviruses and phage. *Nucleic Acids Res* **42**: 9096-9107

Sandbaumhüter M, Döhner K, Schipke J, Binz A, Pohlmann A, Sodeik B, & Bauerfeind R (2013) Cytosolic herpes simplex virus capsids not only require binding inner tegument protein pUL36 but also pUL37 for active transport prior to secondary envelopment. *Cell Microbiol* **15**: 248-269

Schilling M, Bulli L, Weigang S, Graf L, Naumann S, Patzina C, Wagner V, Bauersfeld L, Goujon C, Hengel H, Halenius A, Ruzsics Z, Schaller T, & Kochs G (2018) Human MxB Protein Is a Pan-herpesvirus Restriction Factor. *J Virol* **92**: 10.1128/JVI.01056-18. Print 2018 Sep 1

Schipke J, Pohlmann A, Diestel R, Binz A, Rudolph K, Nagel CH, Bauerfeind R, & Sodeik B (2012) The C terminus of the large tegument protein pUL36 contains multiple capsid binding sites that function differently during assembly and cell entry of herpes simplex virus. *J Virol* **86**: 3682-3700

Schneider SM, Lee BH, & Nicola AV (2021) Viral entry and the ubiquitin-proteasome system. *Cell Microbiol* **23**: e13276

Schulte B, Buffone C, Opp S, Di Nunzio F, De Souza Aranha Vieira, D. A., Brandariz-Nunez A, & Diaz-Griffero F (2015) Restriction of HIV-1 Requires the N-Terminal Region of MxB as a Capsid-Binding Motif but Not as a Nuclear Localization Signal. *J Virol* **89**: 8599-8610

Shannon P, Markiel A, Ozier O, Baliga NS, Wang JT, Ramage D, Amin N, Schwikowski B, & Ideker T (2003) Cytoscape: a software environment for integrated models of biomolecular interaction networks. *Genome Res* **13**: 2498-2504

Smaga SS, Xu C, Summers BJ, Digianantonio KM, Perilla JR, & Xiong Y (2019) MxB Restricts HIV-1 by Targeting the Tri-hexamer Interface of the Viral Capsid. *Structure* **27**: 1234-1245.e5

Snijder J, Radtke K, Anderson F, Scholtes L, Corradini E, Baines J, Heck AJR, Wuite GJL, Sodeik B, & Roos WH (2017) Vertex-Specific Proteins pUL17 and pUL25 Mechanically Reinforce Herpes Simplex Virus Capsids. *J Virol* **91**: 10.1128/JVI.00123-17. Print 2017 Jun 15

Stempel M, Chan B, & Brinkmann MM (2019) Coevolution pays off: Herpesviruses have the license to escape the DNA sensing pathway. *Med Microbiol Immunol* **208**: 495-512

Sumner RP, Harrison L, Touizer E, Peacock TP, Spencer M, Zuliani-Alvarez L, & Towers GJ (2020) Disrupting HIV-1 capsid formation causes cGAS sensing of viral DNA. *EMBO J* **39**: e103958

Sun C, Luecke S, Bodda C, Jonsson KL, Cai Y, Zhang BC, Jensen SB, Nordentoft I, Jensen JM, Jakobsen MR, & Paludan SR (2019) Cellular Requirements for Sensing and Elimination of Incoming HSV-1 DNA and Capsids. *J Interferon Cytokine Res* **39**: 191-204

Szklarczyk D, Gable AL, Lyon D, Junge A, Wyder S, Huerta-Cepas J, Simonovic M, Doncheva NT, Morris JH, Bork P, Jensen LJ, & Mering CV (2019) STRING v11: protein-protein association networks with increased coverage, supporting functional discovery in genome-wide experimental datasets. *Nucleic Acids Res* **47**: D607-D613

Temple J, Tripler TN, Shen Q, & Xiong Y (2020) A snapshot of HIV-1 capsid-host interactions. *Curr Res Struct Biol* **2**: 222-228

Tsuchiya S, Yamabe M, Yamaguchi Y, Kobayashi Y, Konno T, & Tada K (1980) Establishment and characterization of a human acute monocytic leukemia cell line (THP-1). *Int J Cancer* **26**: 171-176

Turan A, Grosche L, Krawczyk A, Muhl-Zurbes P, Drassner C, Duthorn A, Kummer M, Hasenberg M, Voortmann S, Jastrow H, Dorrie J, Schaft N, Kraner M, Döhner K, Sodeik B, Steinkasserer A, & Heilingloh CS (2019) Autophagic degradation of lamins facilitates the nuclear egress of herpes simplex virus type 1. *J Cell Biol* **218**: 508-523

Tyanova S, Temu T, & Cox J (2016) The MaxQuant computational platform for mass spectrometry-based shotgun proteomics. *Nat Protoc* **11**: 2301-2319

876 Tyanova S, Temu T, Sinitcyn P, Carlson A, Hein MY, Geiger T, Mann M, & Cox J (2016) The Perseus
877 computational platform for comprehensive analysis of (prote)omics data. *Nat Methods* **13**: 731-
878 740

879 Vasudevan AAJ, Bahr A, Grothmann R, Singer A, Haussinger D, Zimmermann A, & Munk C (2018) MXB
880 inhibits murine cytomegalovirus. *Virology* **522**: 158-167

881 Warner MS, Geraghty RJ, Martinez WM, Montgomery RI, Whitbeck JC, Xu R, Eisenberg RJ, Cohen GH,
882 & Spear PG (1998) A cell surface protein with herpesvirus entry activity (HveB) confers
883 susceptibility to infection by mutants of herpes simplex virus type 1, herpes simplex virus type 2,
884 and pseudorabies virus. *Virology* **246**: 179-189

885 Whitley R & Johnston C (2021) Herpes Simplex Viruses: Pathogenesis and Clinical Insights. In *Fields*
886 *Virology: DNA Viruses,* Howley PM, Knipe DM, Cohen JL, Damania BA (eds) pp 297-323. Wolters
887 Kluwer Health/Lippincott Williams & Wilkins; 7th edition (May 17, 2021)

888 Whitley R & Roizman B (2016) Herpes Simplex Viruses. In *Clinical Virology, Fourth Edition,* Richman
889 DD, Whitley RJ, Hayden FJ (eds) pp 415-445. ASM Press

890 Wolfstein A, Nagel CH, Radtke K, Döhner K, Allan VJ, & Sodeik B (2006) The inner tegument promotes
891 herpes simplex virus capsid motility along microtubules in vitro. *Traffic* **7**: 227-237

892 Xie L, Ju Z, Zhong C, Wu Y, Zan Y, Hou W, & Feng Y (2021) GTPase Activity of MxB Contributes to Its
893 Nuclear Location, Interaction with Nucleoporins and Anti-HIV-1 Activity. *Virol Sin* **36**: 85-94

894 Zenner HL, Yoshimura S, Barr FA, & Crump CM (2011) Analysis of Rab GTPase-activating proteins
895 indicates that Rab1a/b and Rab43 are important for herpes simplex virus 1 secondary
896 envelopment. *J Virol* **85**: 8012-8021

897 Zhang Y & McKnight JL (1993) Herpes simplex virus type 1 UL46 and UL47 deletion mutants lack VP11
898 and VP12 or VP13 and VP14, respectively, and exhibit altered viral thymidine kinase expression. *J*
899 *Virol* **67**: 1482-1492

900 Zhang Z, Kim T, Bao M, Facchinetti V, Jung SY, Ghaffari AA, Qin J, Cheng G, & Liu YJ (2011) DDX1,
901 DDX21, and DHX36 helicases form a complex with the adaptor molecule TRIF to sense dsRNA in
902 dendritic cells. *Immunity* **34**: 866-878

903

TABLE LEGENDS

Supplementary Table S1: Host proteins in THP-1 cytosols. Intensity-Based Absolute Quantitation (iBAQ) counts of the host proteins identified in the proteomic analysis of the cytosolic extracts prepared from rested or IFN-induced THP-1 ϕ cytosol. Statistical analyses were performed with a Welch's t-test. The following cut-offs were set for differentially-expressed proteins: permutation-based false-discovery rate ≤ 0.05 and $|\log_2$ fold-change$| \geq 0.5$. The protein groups were filtered to keep only the intensities measured in at least three out of four replicates per condition. Gene Ontology knowledge was used to reference the proteins previously described as induced by interferon.

Supplementary Table S2: Host proteins in capsid-host protein complexes. Intensity-Based Absolute Quantitation (iBAQ) counts of host proteins identified in the $V_{0.1}$, $V_{0.5}$, V_1 and D capsid-host protein complexes assembled in rested or IFN-induced THP-1 ϕ cytosol. Statistical analyses were performed with a Welch's t-test. The following cut-offs were set for differentially expressed proteins: permutation-based false-discovery rate ≤ 0.05 and a $|\log_2$ fold-change $\geq 1.5|$. The protein groups were filtered to keep only those with intensities measured in at least three out of four replicates, in at least one condition. "Interaction significance" column indicates the proteins considered as specific interactors.

Supplementary Table S3: Viral proteins in capsid-host protein complexes. Intensity-based absolute quantification (iBAQ) counts of HSV-1(17^+)Lox viral proteins from isolated $V_{0.1}$, $V_{0.5}$, V_1 and D capsids (A) normalized to the intensity of the major capsid protein VP5, (B) unnormalized LFQ intensities. The viral proteins were filtered to keep only those with intensities measured in at least three out of four replicates, in at least one condition.

Supplementary Table S4: List of Antibodies. mAb: monoclonal antibody. pAb: polyclonal antibody.

929 # TABLE S4: LIST OF ANTIBODIES

Antigen	Name	species, type	Source and Reference
HSV-1 proteins			
capsid	SY4563	rabbit pAb	(Döhner *et al.*, 2018)
VP5	NC-1	rabbit mAb	Gary Cohen & Roselyn Eisenberg, University of Pennsylvania, Philadelphia, USA; (Cohen, G. H. *et al.*, 1980)
Host proteins			
nuclear pore	mAb414	mouse mAb	ab24609, Abcam
p230	p230	mouse mAb	611280, BD Biosciences
E-cadherin	α-E-cadherin	mouse mAb	C37020;610404, BD Transduction Laboratories
calnexin	α-calnexin	rabbit pAb	Ari Helenius, ETH Zürich, Switzerland; (Hammond & Helenius, 1994)
Tom20	F-10	mouse mAb	Sc-17764, Santa Cruz Biotechnology
GAPDH	14C10	rabbit pAb	2118S, Cell Signaling (NEB)
MxA/MxB	M143	mouse mAb	(Flohr *et al.*, 1999)
MxA	α-Mx1	rabbit pAb	ab207414, Abcam
MxB	α-Mx2	rabbit pAb	NBP1-81018, Novus Biological
FLAG	ANTI-FLAG	rabbit pAb	F7425, Sigma-Aldrich

930

FIGURES

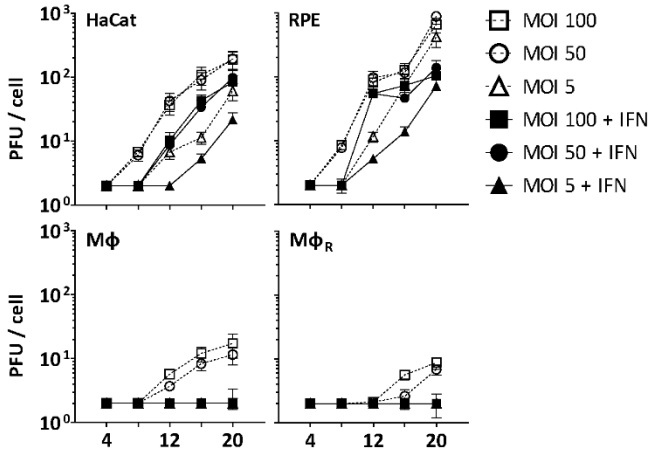

Figure 1: IFN restricts HSV-1 infection in keratinocytes, epithelial cells, and macrophages. HaCat, RPE, Mϕ, or $M\phi_R$ cells were mock-treated or treated with human IFN-α (1000 U/mL) for 16 h and were infected with HSV-1(17$^+$)Lox at 2.5 × 106 (MOI 5), 2.5 × 107 (MOI 50), or 5 × 107 PFU/mL (MOI 100), and the amount of cell-associated and extracellular virions was titrated on Vero cells. Each data point represents the mean of the three technical replicates of the combined cell-associated and extracellular titers. The error bars represent the standard deviation.

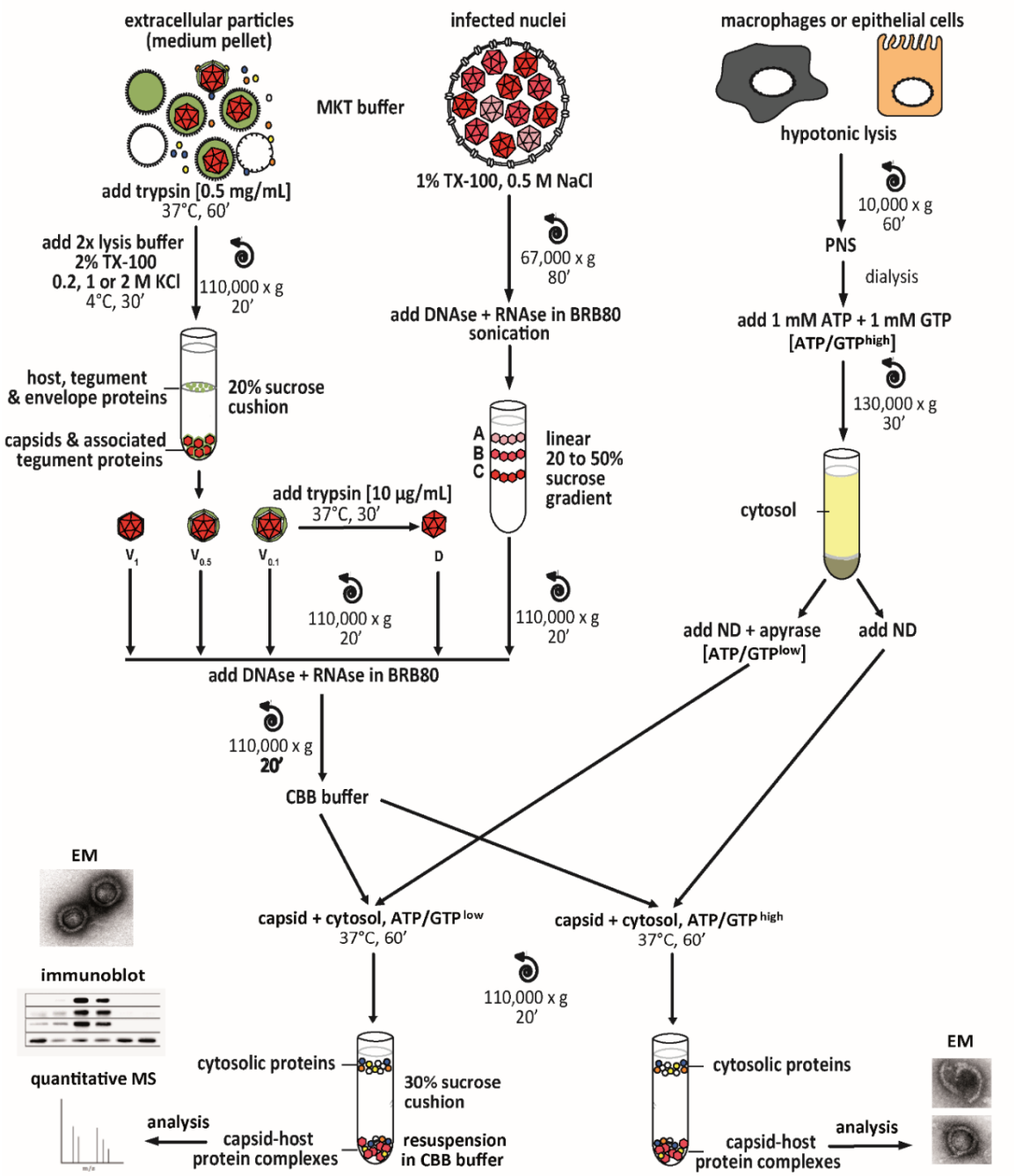

940

941 ***Supplementary Figure S1: Experimental strategy to generate host protein-capsid complexes.***
942 Tegumented viral $V_{0.1}$, $V_{0.5}$, or V_1 capsids (red) were isolated from extracellular particles released from
943 BHK-21 cells infected with HSV-1(17$^+$)Lox. They were lysed in 1% Triton X-100 to solubilize the viral
944 envelope, and to extract different amounts of tegument (green) in the presence of 0.1 M, 0.5 M or
945 1 M KCl. D capsids were generated from $V_{0.1}$ capsids by mild trypsin digestion. These different capsid
946 types were purified through sucrose cushions. Tegument-free nuclear A, B, and C capsids were
947 isolated from the nuclei of BHK cells infected with HSV-1(17$^+$)Lox by gradient sedimentation. The
948 capsids were resuspended in BRB80 buffer, treated with benzonase to degrade DNA and RNA,
949 sedimented again, and incubated with cytosol fractions (yellow) from control or IFN-induced
950 macrophages (THP-1 ϕ) or epithelial A549 cells. After sedimentation through sucrose cushions, the
951 capsid-host protein complexes were analysed by mass spectrometry (MS), immunoblot, or electron
952 microscopy (EM). PNS, post-nuclear-supernatant; ND, nocodazole.

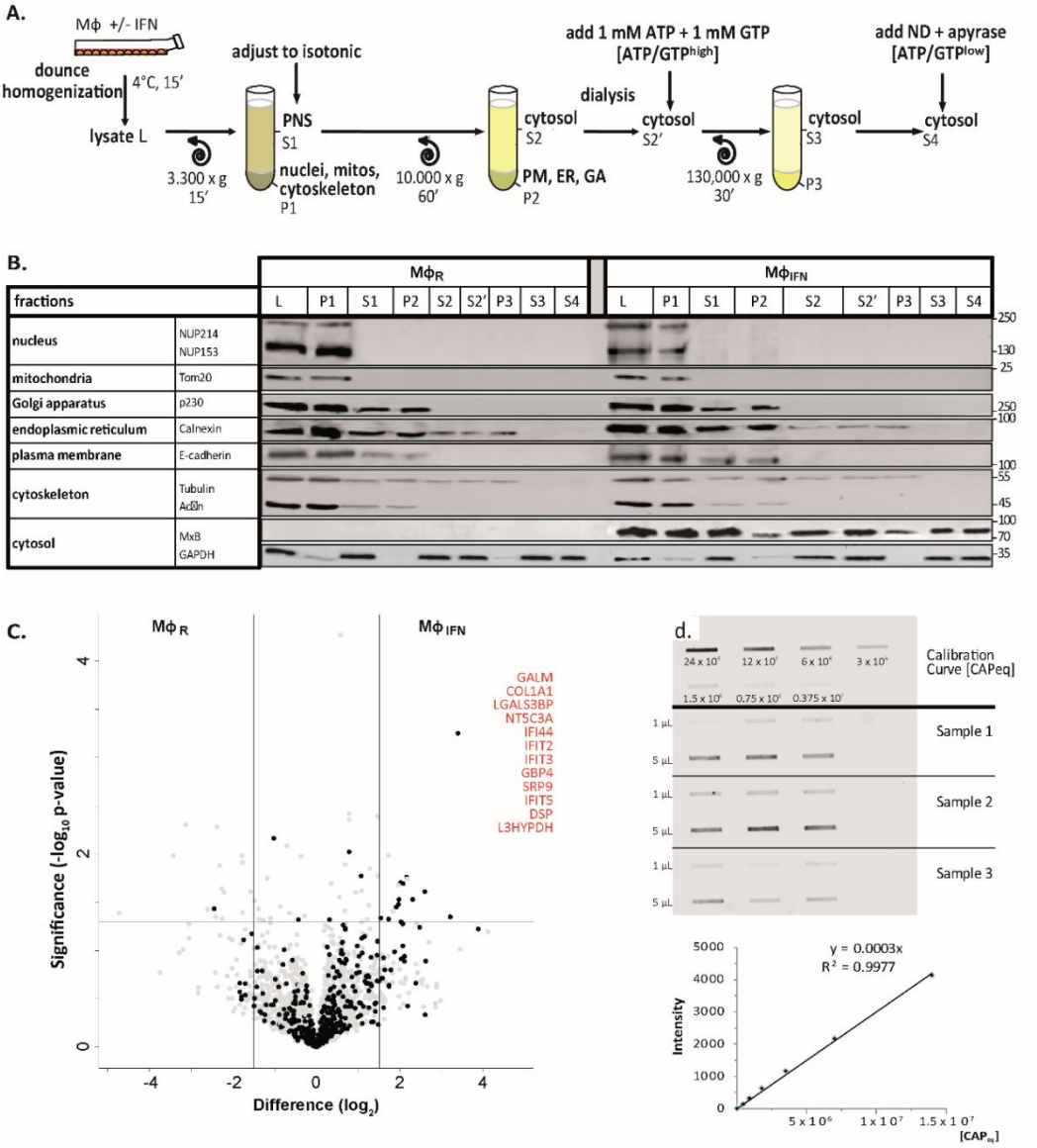

953

954 ***Supplementary Figure S2: Characterization of cytosolic extracts and calibration of capsids.*** (A)
955 Cytosols were prepared from rested $M\phi_R$ or IFN-induced $M\phi_{IFN}$ macrophage cells. After swelling in
956 hypotonic buffer, the cells were homogenized (L), and nuclei and mitochondria were sedimented
957 (P1). The post-nuclear supernatant (S1) was adjusted to isotonic salt concentration, and centrifuged
958 to sediment membrane compartments (P2), like the PM, ER and GA. To control the nucleotide
959 concentration, the cytosols (S2) were dialyzed against a 7 kDa membrane prior to the addition of an
960 ATP regeneration system (S2'). The remaining actin filaments and microtubules were sedimented in
961 P3 to obtain a soluble cytosol fraction (S3). To reduce ATP and GTP levels, some cytosols were
962 treated with 10 U/mL of apyrase (S4). Nocodazole (ND) was added to prevent polymerization and
963 sedimentation of microtubules. (B) All fractions generated were analysed by immunoblot for the
964 respective compartment marker proteins as indicated. Nup, nucleoporins. (C) Volcano plot
965 summarizing the effect of IFN induction on the cytosol proteome. ISGs associated with the
966 interferomeDB were enriched in cytosol from $M\phi_{IFN}$ as compared to $M\phi_R$ with an FDR of 7.96×10^{-7}
967 and an FC ≥ 2 in at least 1 experiment (Fisher's exact test). IFN-inducible proteins are indicated by
968 black circles, and those with an abundance $\log_2$ difference ≥ 1.5 (vertical lines), and an uncorrected p-
969 value < 0.05 (horizontal line) are labelled in red. (D) The slot blot used for the estimation of capsid
970 concentrations (capsids equivalent; CAP_{eq}) of all preparations was labeled with anti-capsid antibodies
971 (rabbit pAb SY4563) and adjusted to a calibration curve of a standard preparation.

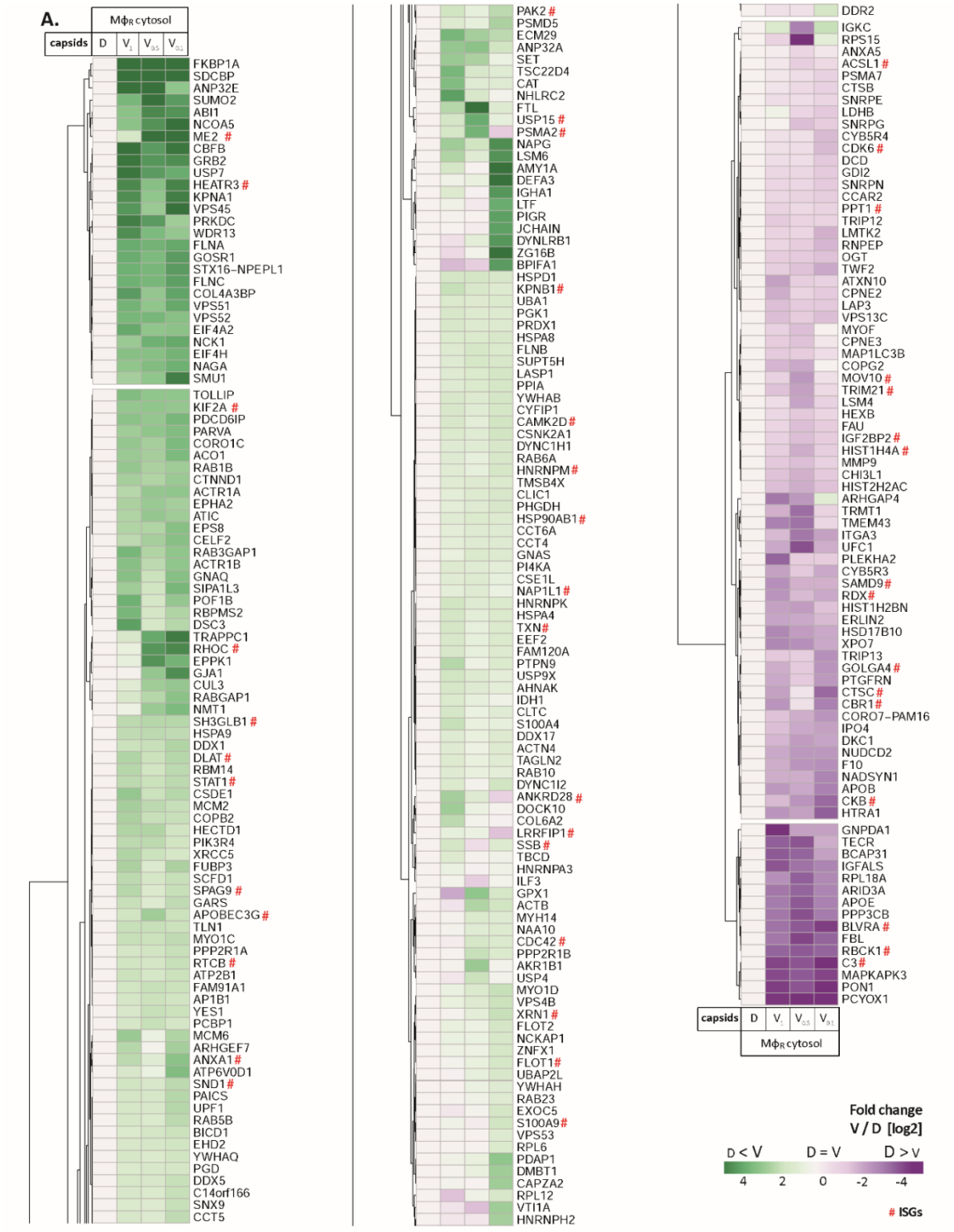

Supplementary Figure S3A: HSV-1 capsids interactomes. Unbiased hierarchical clustered heat map showing the $\log_2$ fold changes of host proteins identified from capsids-host protein sediments (c.f. Fig. 2; abundance $\log_2$ difference larger than 1; significance permutation-based FDR smaller than 0.05) from (A) cytosol of resting Mϕ, or (B) IFN-induced $M\phi_{IFN}$ macrophages. For each protein, the fold change was calculated based on their abundance (iBAQs) in V_1, $V_{0.5}$, or $V_{0.1}$ capsids compared to D capsids using a linear scale from violet being the lowest to dark green being the highest.

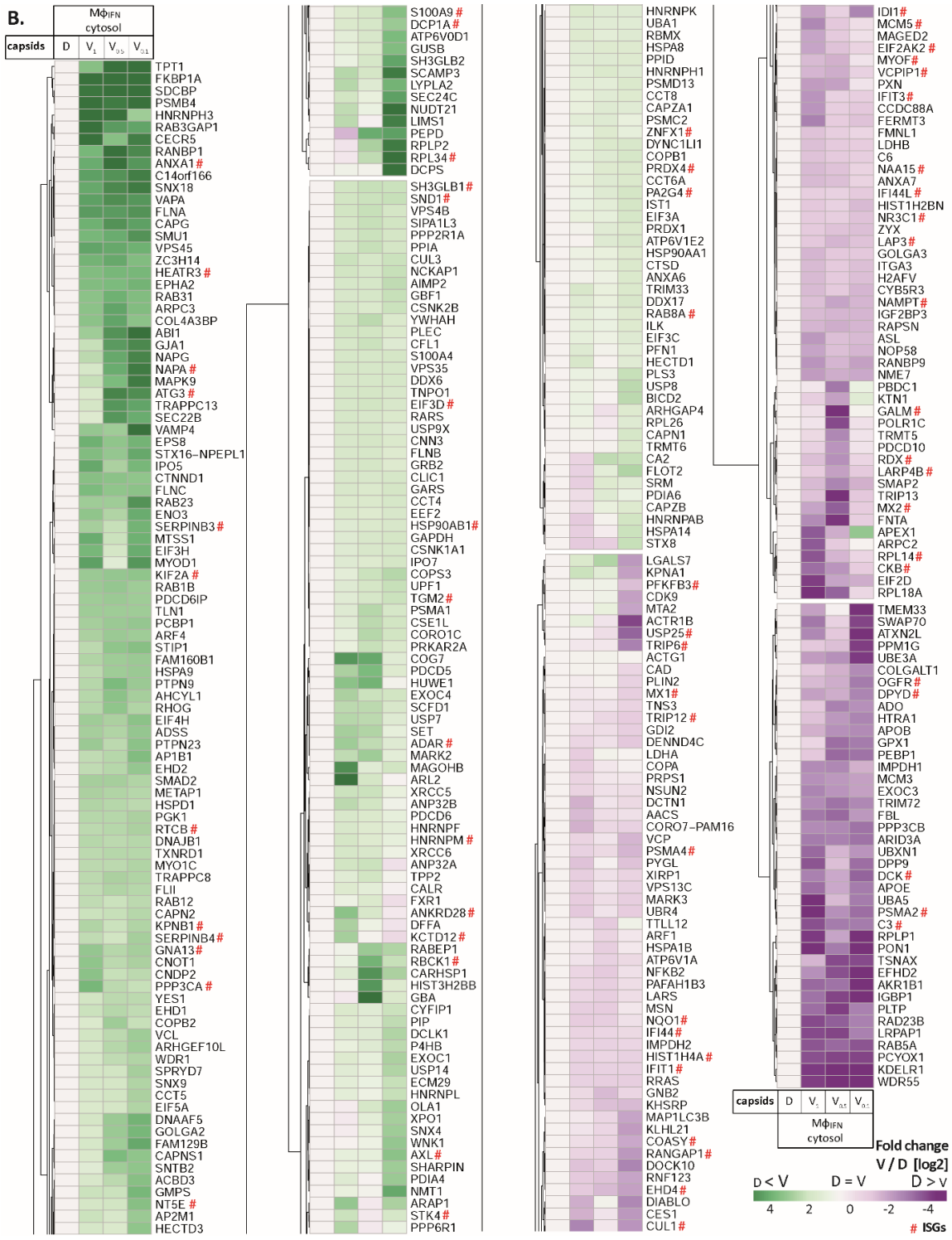

Supplementary Figure S3B: HSV-1 capsids interactomes. Unbiased hierarchical clustered heat map showing the $\log_2$ fold changes of host proteins identified from capsids-host protein sediments (c.f. Fig. 2; abundance $\log_2$ difference larger than 1; significance permutation-based FDR smaller than 0.05) from (A) cytosol of resting macrophages (M_ϕ), or (B) IFN-induced macrophages ($M_{\phi IFN}$). For each protein, the fold change was calculated based on their abundance (iBAQs) in V_1, $V_{0.5}$, or $V_{0.1}$ capsids compared to D capsids using a linear scale from violet being the lowest to dark green being the highest.

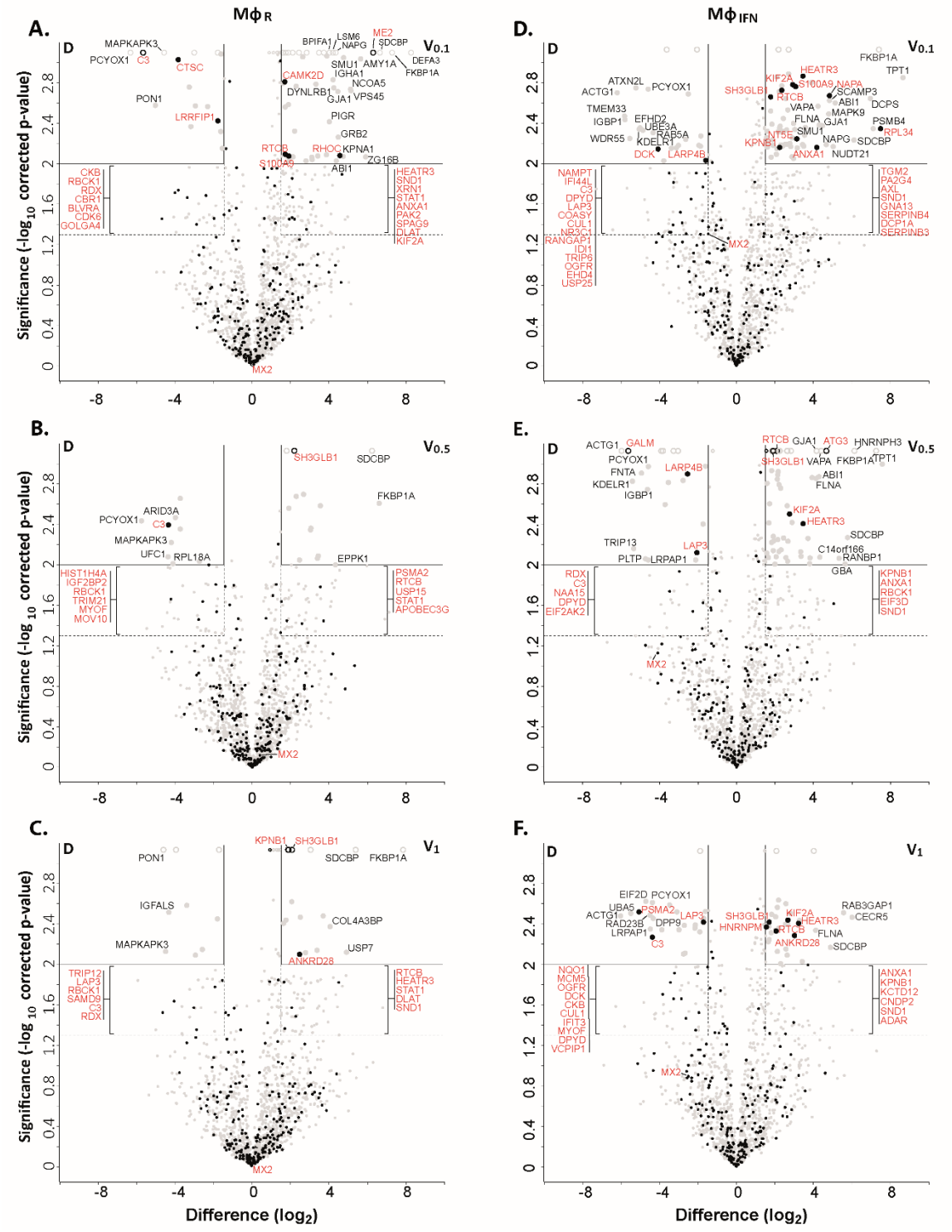

Figure 2: Cytosolic IFN-induced macrophage proteins binding to HSV-1 capsids. Volcano plots of iBAQs counts of proteins identified in capsid-host protein complexes assembled in cytosol from resting THP-1 ϕ cells (A - C) or treated with interferon-α (D - F) using $V_{0.1}$ (A, D), $V_{0.5}$ (B, E), or V_1 (C, F) capsids in comparison to D capsids. Proteins identified as highly specific interactions are indicated with larger symbols (log_2 difference: 1.5; Welch's t-test, two-tailed, permutation-based FDR ≤ 0.01); those with a log_2 difference ≥ 4 are annotated. ISGs (interferome.org) are indicated by filled black circles, and are annotated in red if significantly enriched (permutation-based FDR ≤ 0.05, and log_2 difference ≥ 1.5). Proteins with a q-value = 0 were imputed to - log_{10} q-value = 3.1 (maximum of the graph), and were indicated with empty circles.

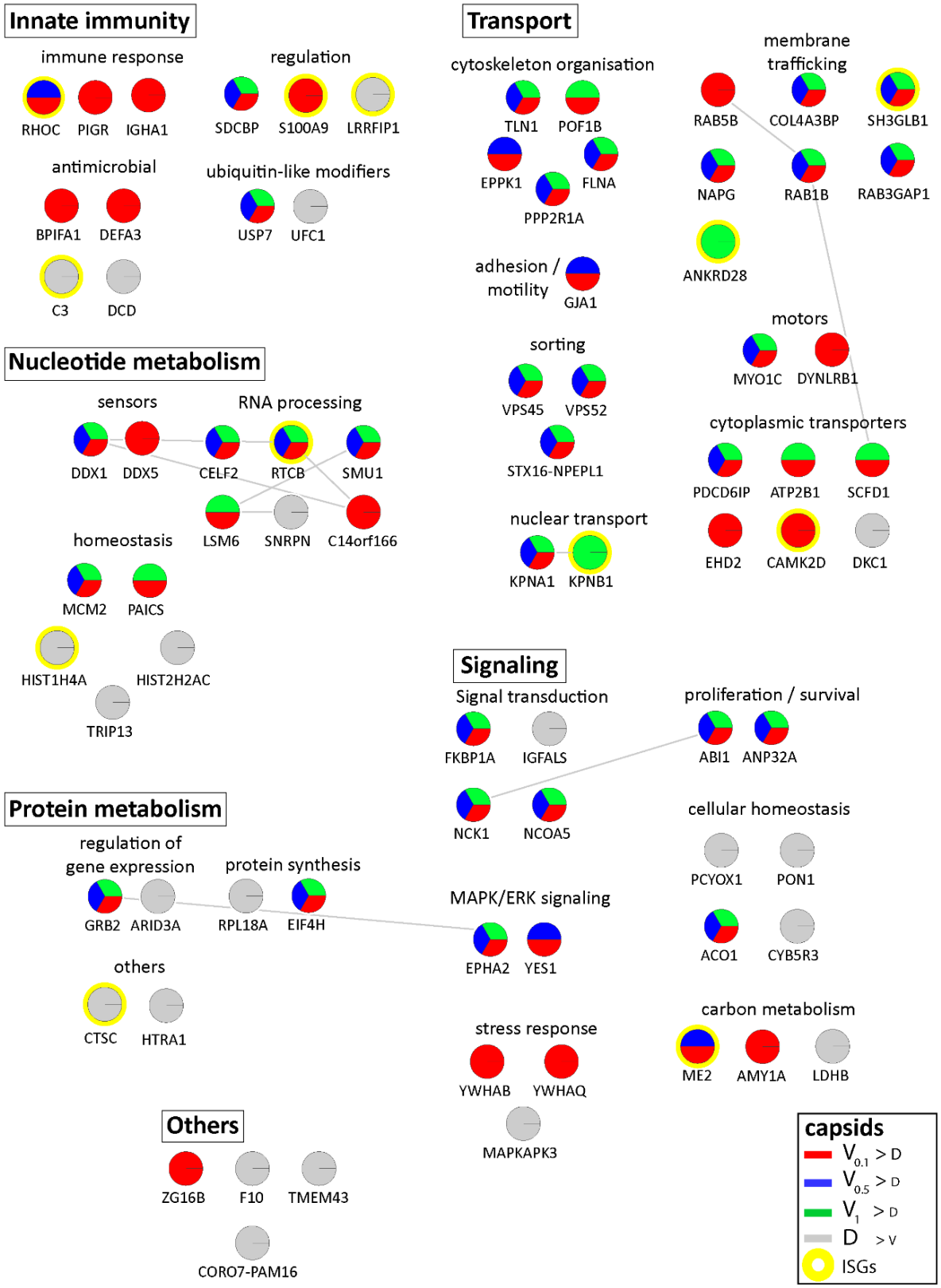

998

999 ***Supplementary Figure S4: Cytosolic proteins of resting macrophage binding to HSV-1 capsids.*** *Host*
1000 proteins from cytosol of resting Mϕ (c.f. Fig. 3A, 3B, 3C; abundance $\log_2$ difference larger than 1.5;
1001 significance permutation-based FDR smaller than 0.05) interacting with $V_{0.1}$, $V_{0.5}$, V_1, or D capsids
1002 were assembled into a functional interaction network of known protein-protein-interactions (grey
1003 lines; STRING database, confidence score of 0.7), and grouped according to their known functions
1004 (Gene Ontology, Pathway analysis). The Pie chart for each protein indicates its relative enrichment on
1005 $V_{0.1}$ (red), $V_{0.5}$ (blue), V_1 (green), or D capsids (grey).

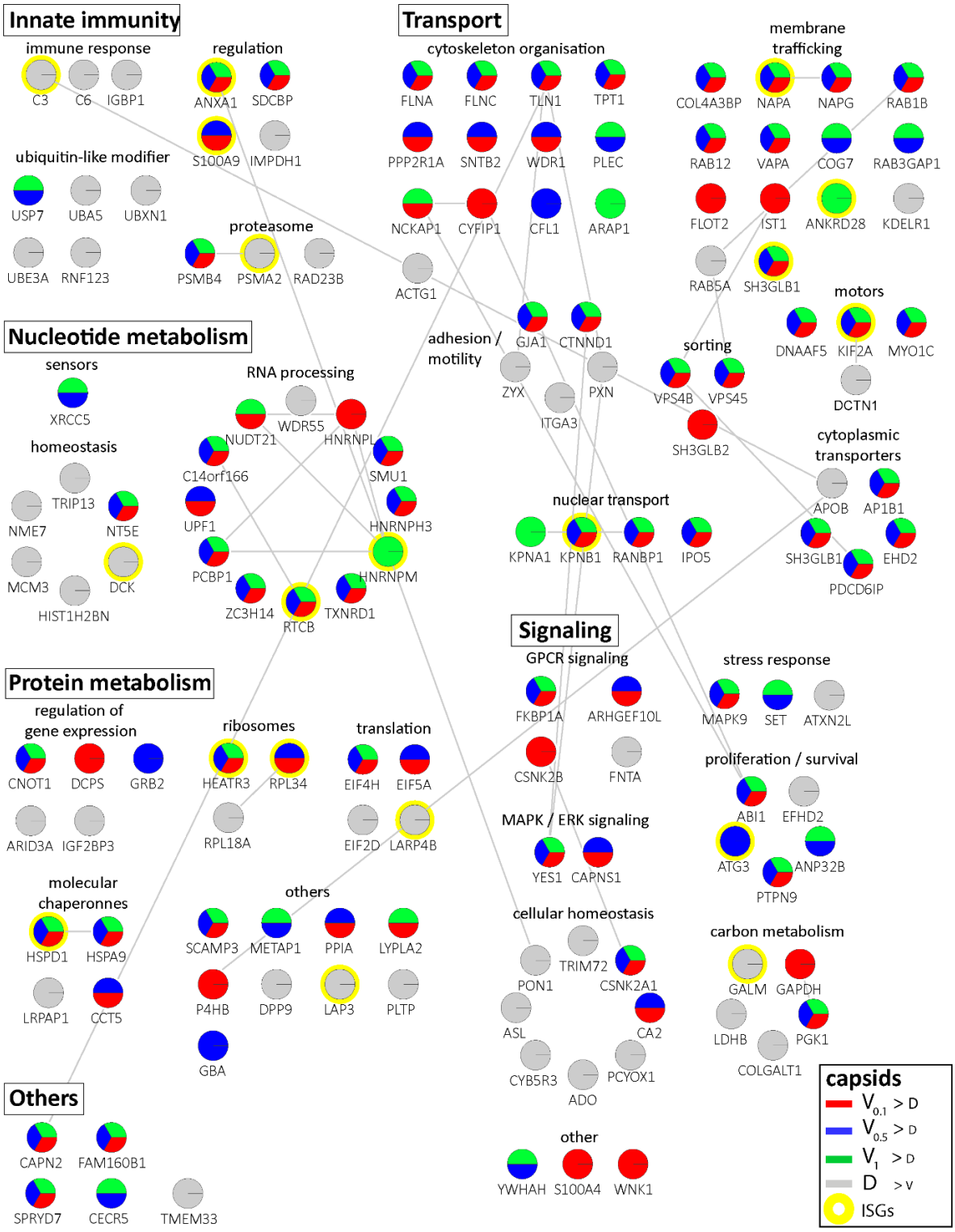

Figure 3: Cytosolic proteins of IFN-induced macrophages binding to HSV-1 capsids. Host proteins from cytosol of IFN-stimulated $M\phi_{IFN}$ (c.f. Fig. 3D, 3E, 3F; abundance $\log_2$ difference larger than 1.5; significance permutation-based FDR smaller than 0.05) interacting with $V_{0.1}$, $V_{0.5}$, V_1, or D capsids were assembled into a functional interaction network of known protein-protein-interactions (grey lines; STRING database, confidence score of 0.7), and grouped according to their known functions (Gene Ontology, Pathway analysis). The Pie chart for each protein indicates its relative enrichment on $V_{0.1}$ (red), $V_{0.5}$ (blue), V_1 (green), or D capsids (grey).

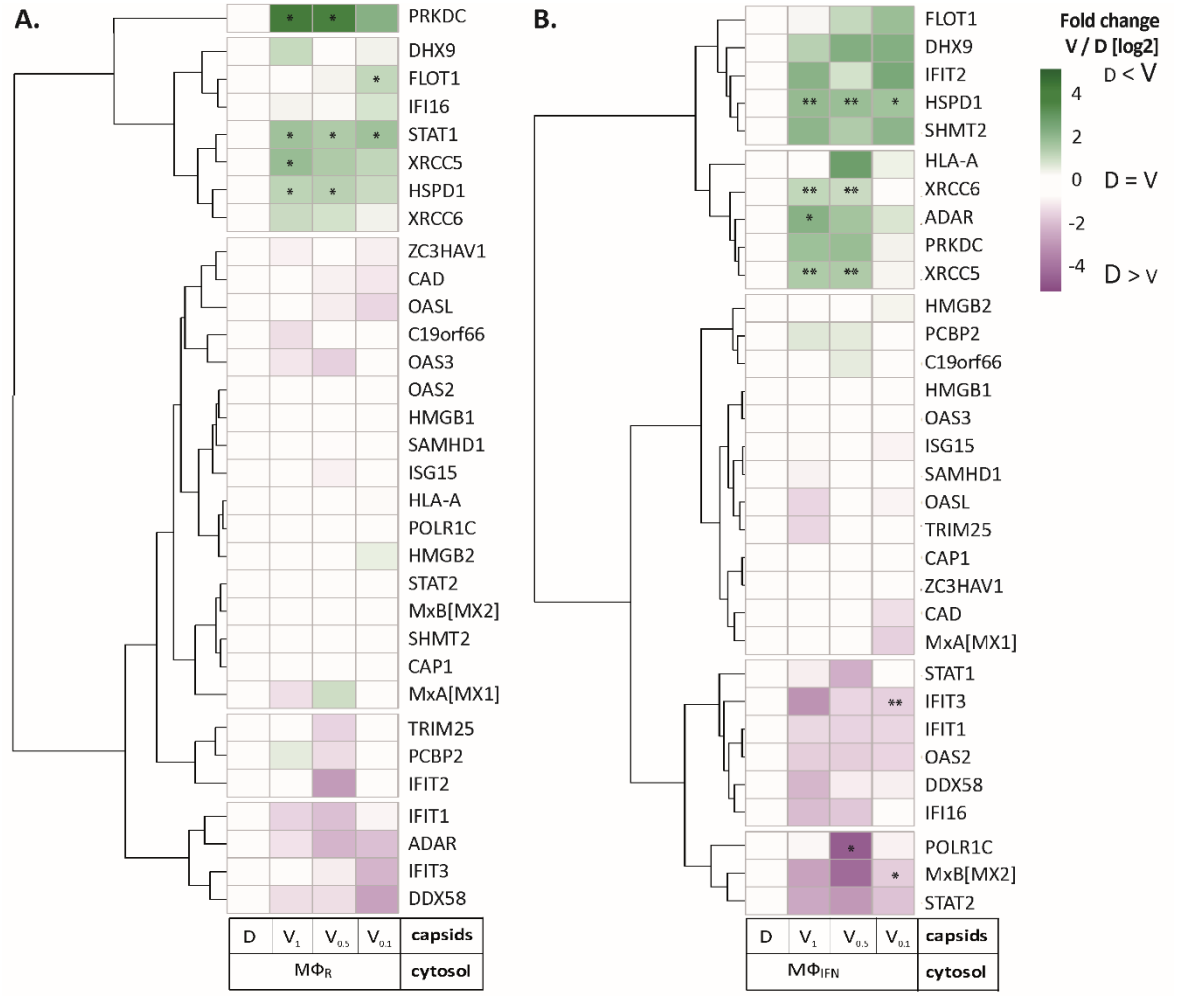

Figure 4: HSV-1 capsids associate with proteins involved in type I IFN response. Unbiased hierarchical clustered heat map showing the $\log_2$ fold changes of IFN-induced proteins (GO type-I IFN) identified from capsids-host protein sediments from cytosol of resting Mϕ, or IFN-induced $M\phi_{IFN}$ macrophages. For each protein, the fold change was calculated based on their abundance (iBAQs) in V_1, $V_{0.5}$ and $V_{0.1}$ capsids as compared to their abundance in D capsids, using a linear scale from violet being the lowest to dark green being the highest. (*) and (**) design the proteins with an FDR corrected p-value < 0.05 and < 0.01, respectively.

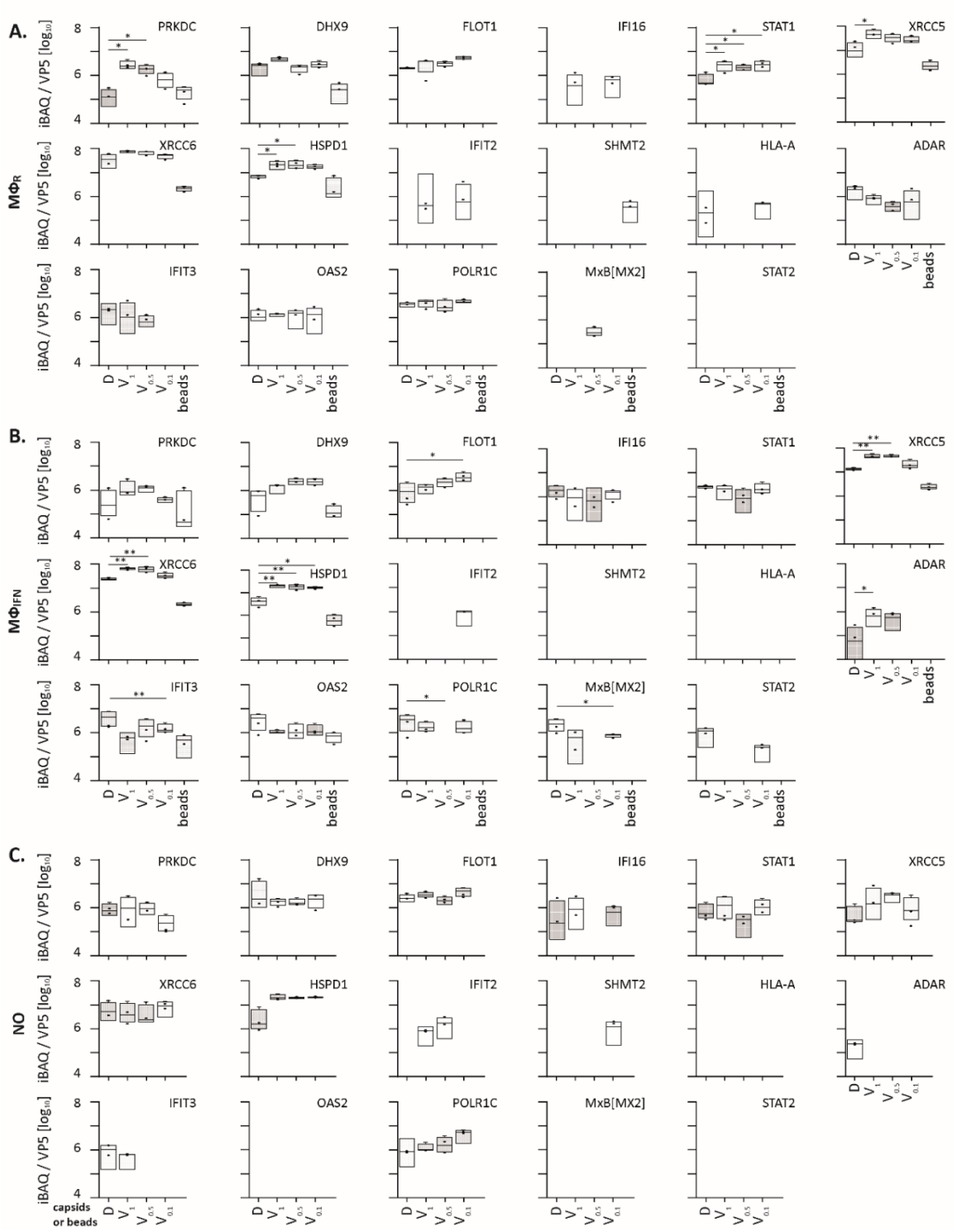

Supplementary Figure S5: HSV-1 capsids binds to a few ISG proteins. Box and whisker plot of iBAQs showing the differential detection of PRKDC, DHX9, FLOT1, IFI16, STAT1, XRCC5, XRCC6, HSPD1, IFIT2, SHMT2, HLA-A, ADAR, IFIT3, OAS2, POLR1C and MX2 in D, V_1, $V_{0.5}$ and $V_{0.1}$ capsids-host protein sediments after incubation in (A) cytosol of resting MΦR macrophages, (B) IFN-induced MΦIFN macrophages or (C) no cytosol. (*) design the significant binding to D or V0.1, V0.5 and V1 capsids as assessed by Welch's t-test (two-tailed, permutation-based FDR ≤ 0.05) comparing D vs $V_{0.1}$, $V_{0.5}$ or V_1 capsids in each cytosol separately.

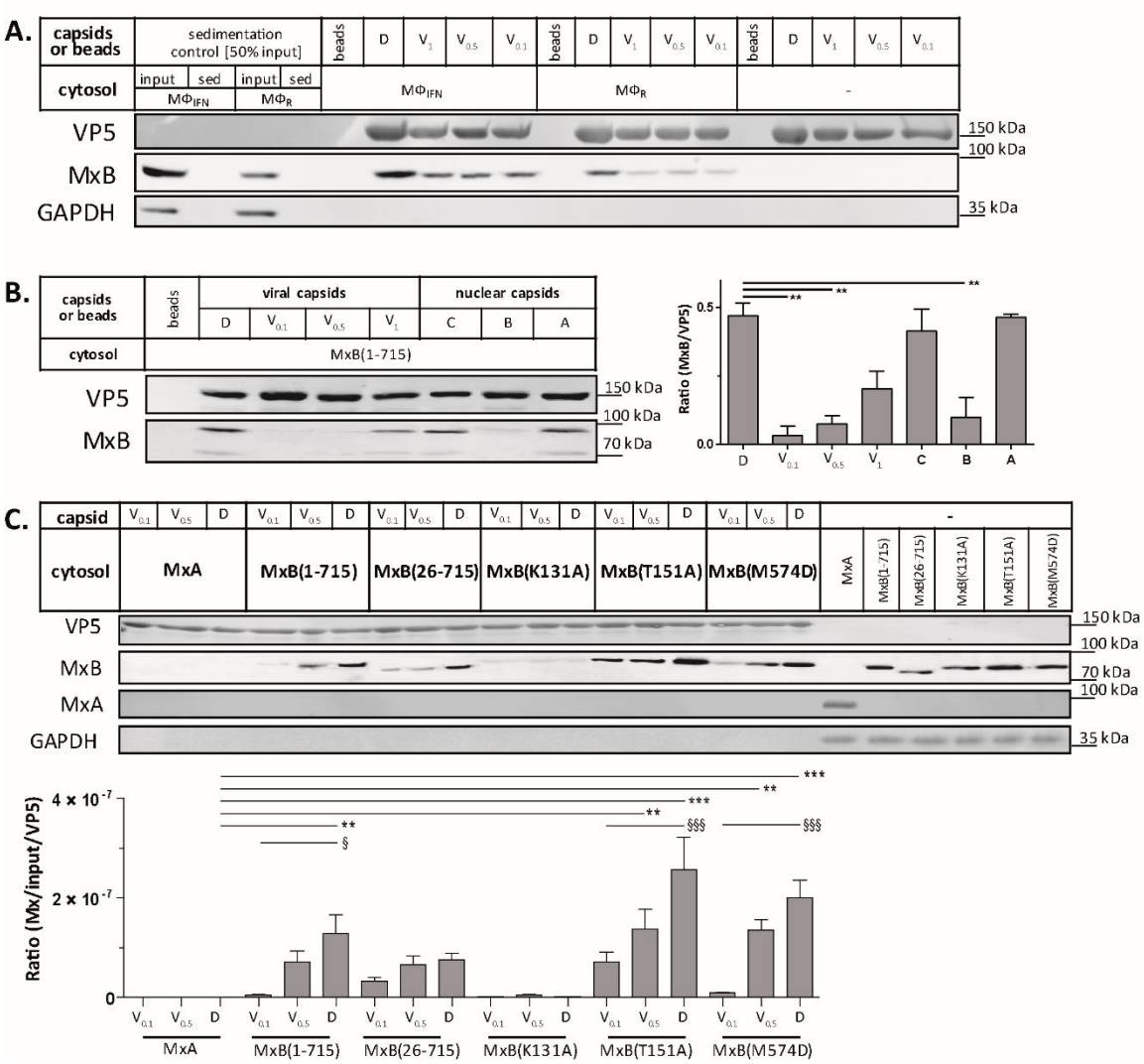

Figure 5: Tegumentation reduces MxB binding to HSV-1 capsids. The binding of MxB to viral $V_{0.1}$, $V_{0.5}$, V_1 or D, or to nuclear A, B or C capsids was analysed after incubation in 0.2 mg/mL cytosol prepared from (A) THP-1 ϕ stimulated or not with IFN, or (B-C) A549 cells stably expressing MxA, MxB(1-715) full length, the short MxB(26-715), or MxB mutants defective in GTP-hydrolysis MxB(T151A), GTP-binding and hydrolysis MxB(K131A), or dimerization MxB(M574D). Sedimented capsid-host protein complexes were then analysed by immunoblot for VP5 (capsid), MxB, MxA and GAPDH as a loading control. As control cytosols were sedimented without capsids (A: sed), or with uncoated agarose beads (A, B: beads). The amounts of MxA/MxB found in the capsid-host protein complexes were quantified, and normalized to their respective VP5 levels. Error bars: SEM. summarized from three experiments. One asterisk denotes $p<0.05$, two asterisks indicate $p<0.01$ and three asterisks represent $p<0.001$ as determined by Welch's t-tests comparisons.

Figure 5A-source data 1-3. Figure 5B-source data 1-3. Figure 5C-source data 1-5. Full western blot images for the corresponding detail sections shown in Figure 5, as well as raw values for western blot quantifications.

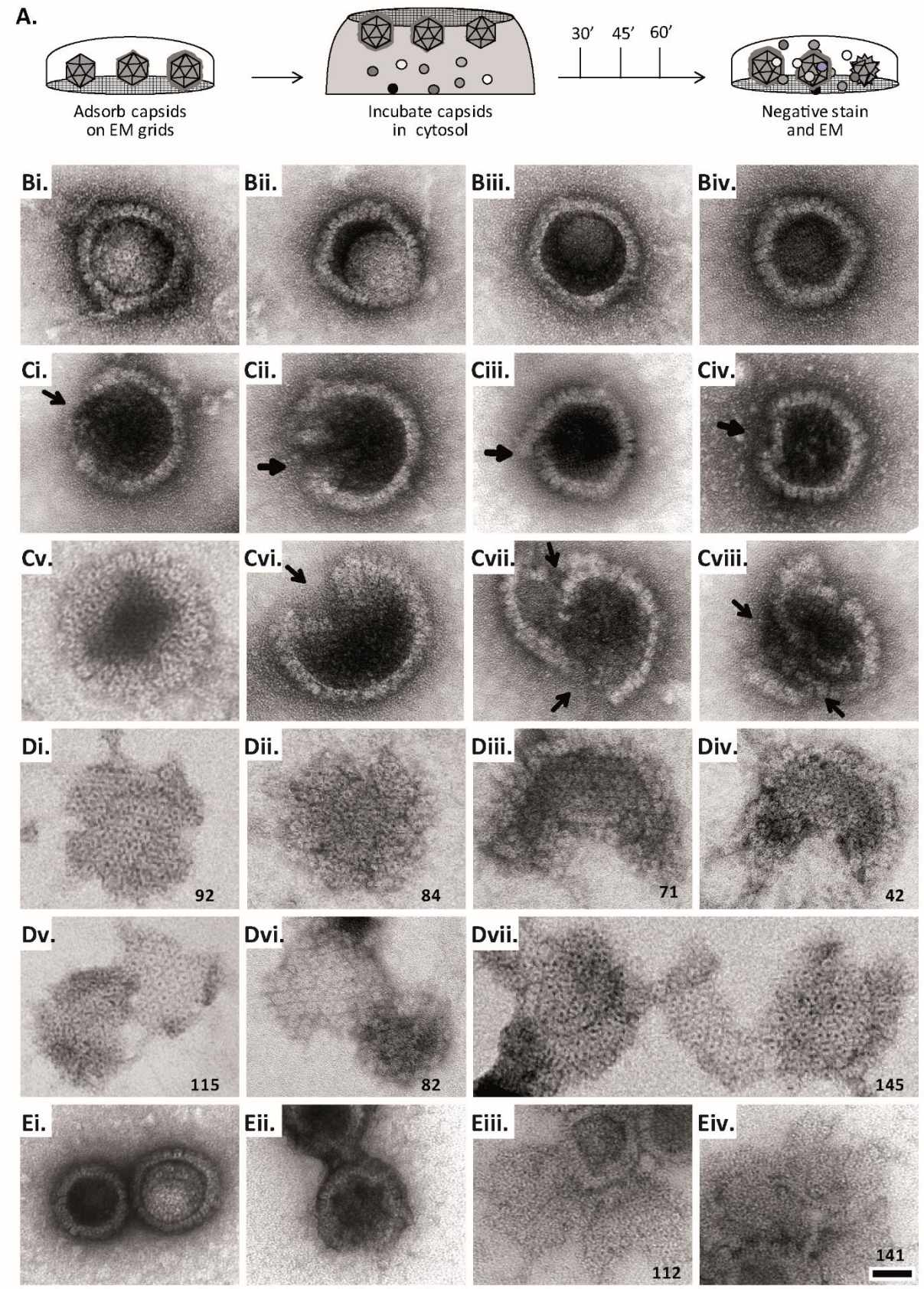

Figure 6: MxB induces disassembly of herpesviral capsids. (A) Experimental design: Capsids were adsorbed onto hydrophilic enhanced carbon-coated EM grids for 20 min at RT. The capsids were incubated in cytosol with ATP/GTP^{high}, and the incubation was stopped at different times by extensive washing. The samples were analysed by EM after negative staining with uranyl acetate. (B-D) Capsids after incubation in cytosol derived from rested Mϕ or IFN-induced Mϕ_{IFN} macrophages, or control or MxB(1-715)

A549 expressing cells for 1 h at 37°C, and classified as (B) intact, (C) punched or (D) disassembled flat phenotypes. The number of capsomers per flat particle was counted, and is displayed at the bottom of each figures. (E) Nuclear VZV capsids remain intact (Ei) after incubation in the cytosol of A549 control cells, or but appear punched (Eii) or as flat shells (Eiii, Eiv) after incubation in the cytosol of A549 cells expressing MxB. Scale bar: 50 nm.

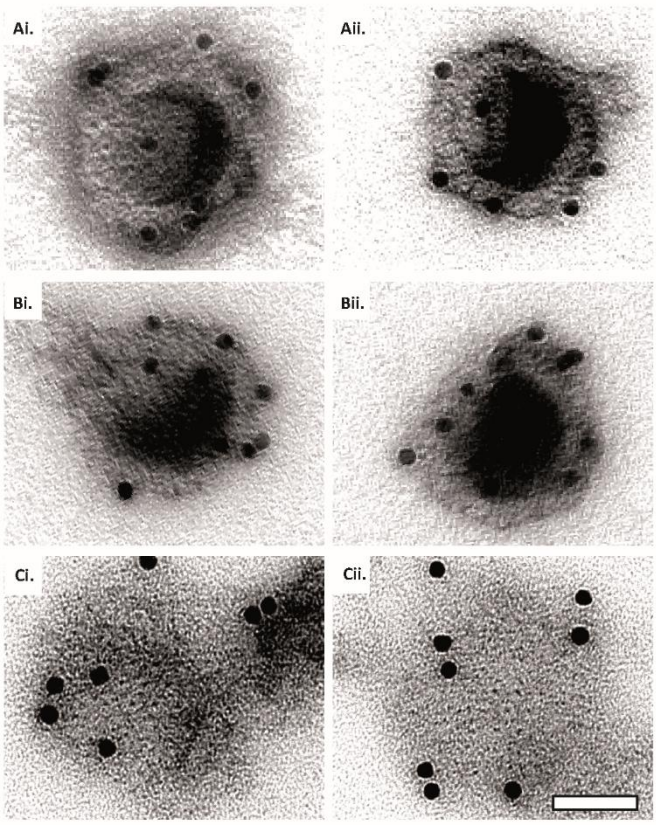

Supplementary Figure S6: Capsid disassembly intermediates by anti-capsid immunoEM. *Images* of capsids after negative staining and labelling with antibodies raised against the major capsid protein VP5 (NC-1), after incubation in ATP-complemented cytosol from A549 control or MxB(1-715) expressing cells for 60 min at 37°C, and classified as (A) *intact*, (B) *punched*, or (C) *flattened* shells. Scale bar: 50 nm.

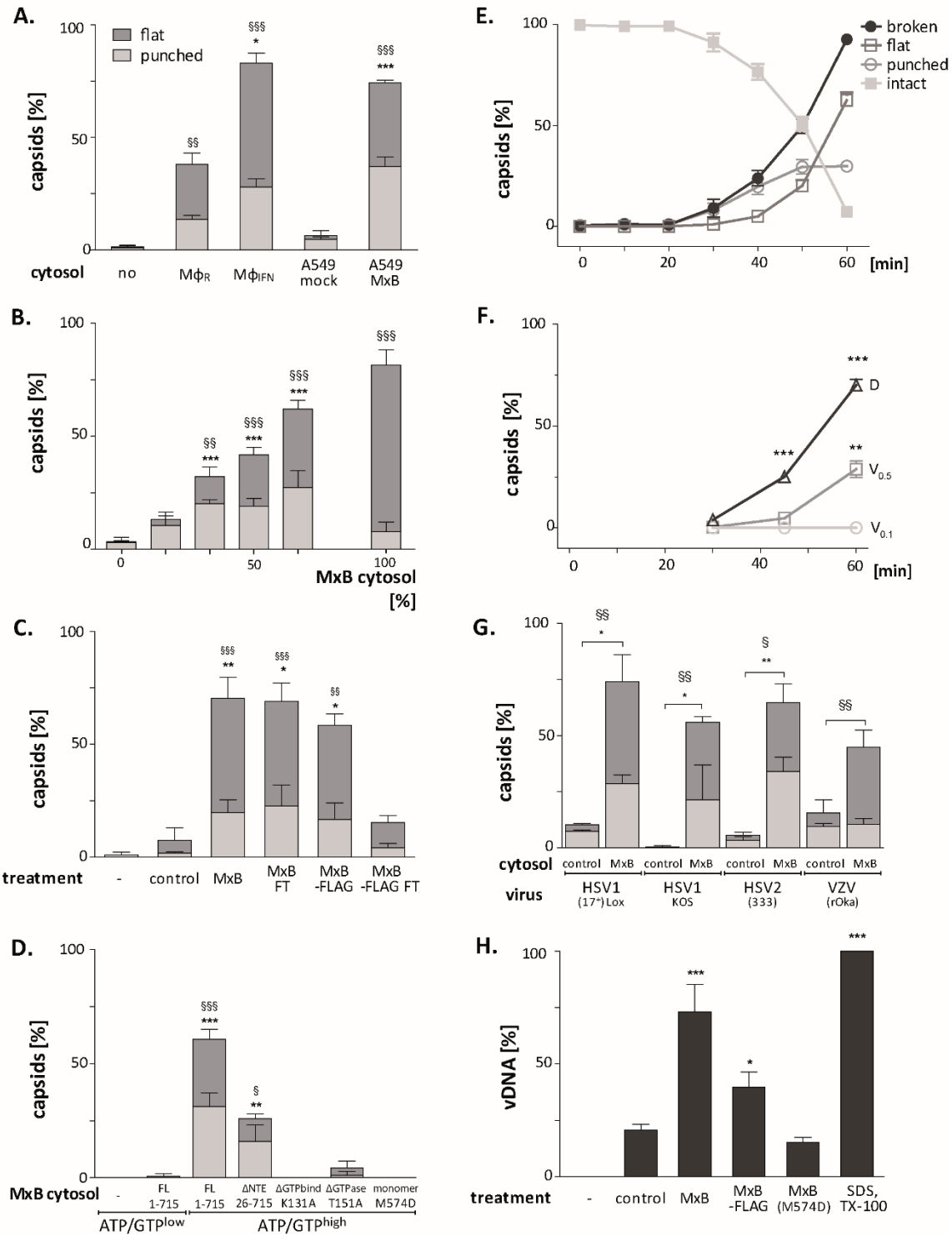

Figure 7: MxB GTP hydrolysis and dimerization required for capsid disassembly and vDNA release of viral genomes. HSV-1 (A-H), HSV-2 (G) or VZV capsids (G) were incubated with cytosol at ATP/GTP^{high} for 1 h or the indicated time (E,F) at 37°C, and classified into *intact, punched* and *flat* capsids by electron microscopy (A-G), or the amount of released viral DNA was measured by qPCR (H). (A) Quantification of *punched* and *flat* D capsid shells in cytosol prepared from rested Mϕ or IFN-induced $M\phi_{IFN}$ macrophages, or from control A549 (mock) or A549-MxB(1-715) cells. (B) Increasing amounts of MxB(1-715) [%] were added to control A549 cytosol, and the amount of *punched* and *flat* capsids were quantified after incubation in these mixtures. (C) Cytosols of A549 cells expressing MxB(1-715) and Mx(25-715) or MxB(1-715)-FLAG and MxB(26-715)-FLAG were incubated with anti-FLAG antibodies coupled to magnetic beads, the flow-through fractions (FT) were harvested, capsids were treated with anti-FLAG treated or control cytosols, and the amount of punched and flat capsids

were quantified. (D) Capsids were incubated in cytosols prepared from A549 cells expressing full-length (FL) MxB(1-715), MxB(26-715), MxB(K131A), MxB(T151A), or MxB(M574D) at ATP/GTP^{low} or ATP/GTP^{high} levels. (E) Time-course of MxB-induced disassembly of capsids pre-adsorbed onto EM grids, incubated with cytosol from A549-MxB(1-715). (F) Analysis of D, $V_{0.5}$, or $V_{0.1}$ capsids treated with MxB(1-175) cytosol for *broken* (*punched + flat*) capsids after negative stain and EM as described for panel E. (G) Quantification of MxB cytosol disassembly of D capsids of HSV-1(17^{+})Lox, HSV-1(KOS), or HSV-2(333), or nuclear C capsids of VZV, after incubation in cytosol from A549-MxB(1-715) cells. (H) D capsids were incubated with different cytosols for 1 h at 37°C or treated with 1% SDS and 10% Tx-100 only, and the released DNA not protected by capsid shells was quantified by qPCR. Error bars: SEM from 100 capsids in 3 biological replicates. One symbol of *or § denotes p<0.05, two p<0.01, and three p<0.001 as determined in One-way analysis of variance with a Bonferroni post-test, and comparing the relative amounts of (*) *punched* and (§) *flat* capsids, or indicating the differences with the mock treated samples (*).

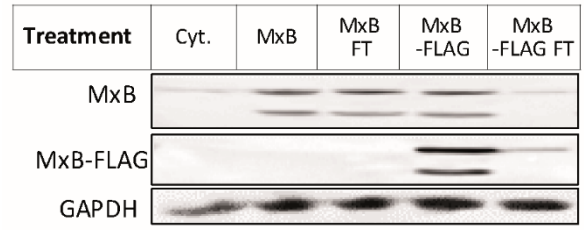

Supplementary Figure S7: Cytosol immunodepleted for MxB. Cytosols prepared from A549-MxB(1-715) and MxB(26-715) expressing MxB(1-715) and MxB(26-715), or A549-MxB-FLAG cells expressing MxB(1-715)-FLAG and MxB(26-715)-FLAG, respectively, were incubated with agarose beads coupled to anti-FLAG antibodies. After immunodepletion with anti-FLAG beads to deplete MxB(1-715)-FLAG and MxB(26-715)-FLAG, the flow through (FT) was harvested. To determine to what extend the FLAG-tagged MxB proteins had been depleted, the starting cytosols (MxB, Mxb-FLAG) as well as the respective FT fractions were probed by immunoblot using antibodies directed against MxB, FLAG, or GAPDH as a loading control.

Figure S7-source data 1,2. Full western blot images for the corresponding detail sections shown in Figure S7.

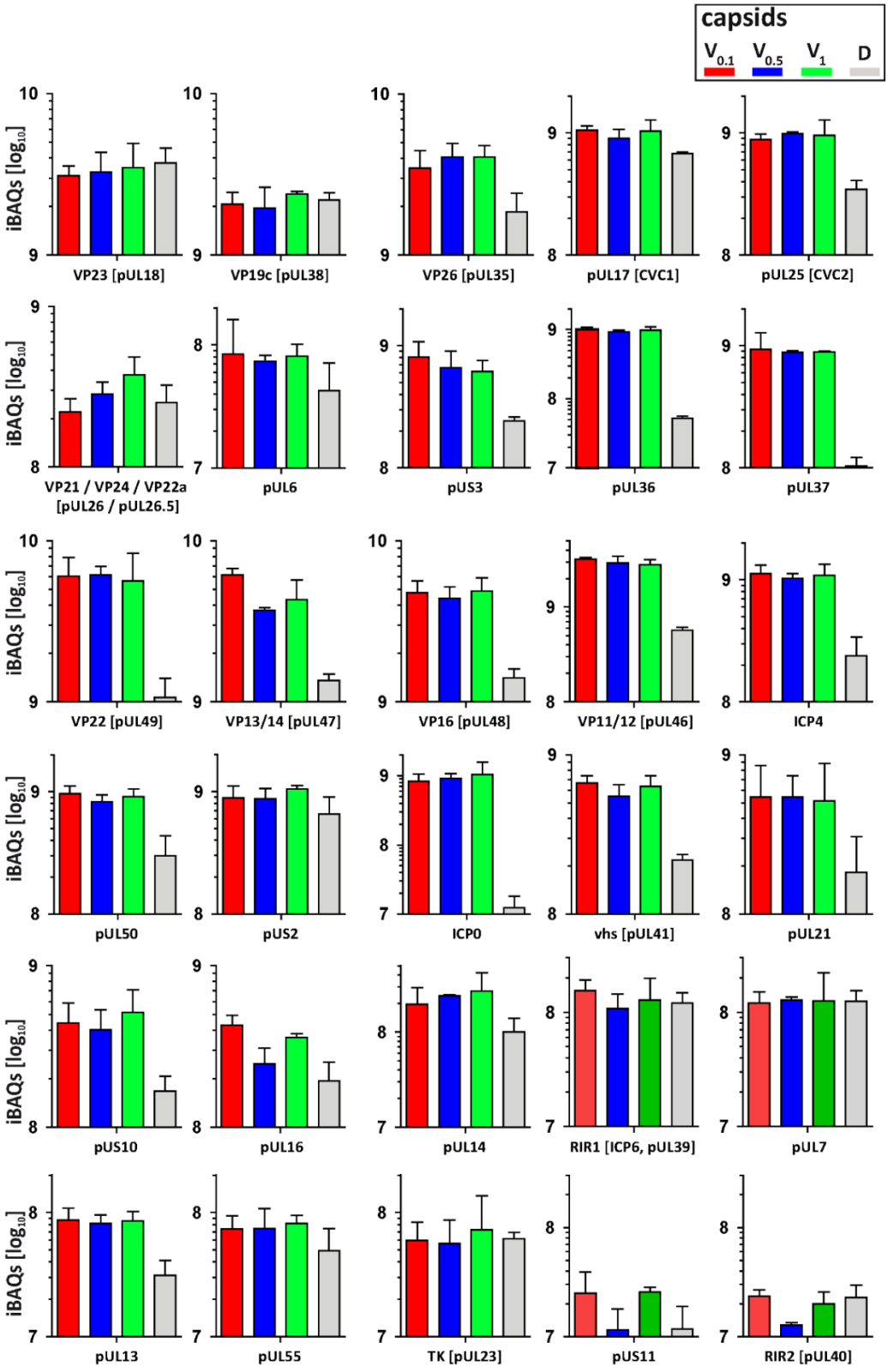

Figure 8: Structural and tegument characterization of $V_{0.1}$, $V_{0.5}$, V_1, and D capsids. The composition of HSV-1(17$^+$)Lox derived $V_{0.1}$ (red), $V_{0.5}$ (blue), V_1 (green) and D (grey) capsids was analysed by quantitative mass spectrometry in four biological replica. The sum of all the peptides intensities (iBAQ, intensity-based absolute quantification) of each viral protein known to participate in the structure of the capsids was normalized to the one of VP5 and displayed in a bar plot for each viral protein.

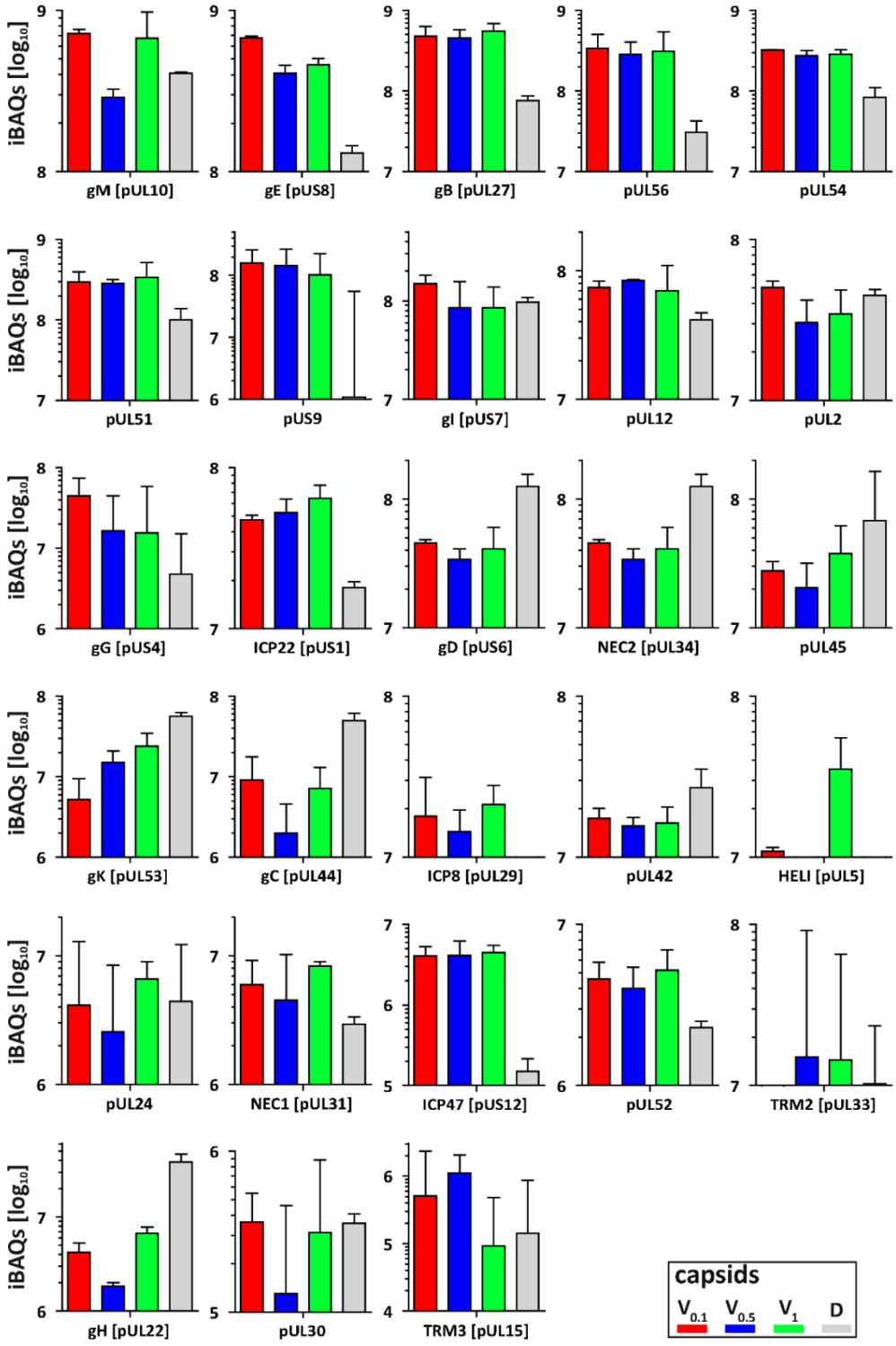

Supplementary Figure S8: Membrane and non-structural proteins on V capsids versus D capsids. The composition of HSV-1 derived $V_{0.1}$ (red), $V_{0.5}$ (blue), V_1 (green) and D (grey) capsids were analysed by quantitative mass spectrometry in four biological replicates. The sum of all the peptides intensities (iBAQ, intensity-based absolute quantification) of each viral protein unknown to participate in the structure of the capsids was normalized to the one of VP5 and displayed in a bar plot